(NASA-CR-165561) STRESS EVALUATIONS UNDER ROLLING/SLIDING CONTACTS Final Report (Battelle Columbus Labs., Ohio.) 54 p HC A04/MF A01 CSCL 20K

NASA CR 165561

N82-17521

Unclas
G3/39 08966

FINAL REPORT

on

STRESS EVALUATIONS UNDER ROLLING/SLIDING CONTACTS

to

NASA

NATIONAL AERONAUTICS AND SPACE ADMINISTRATION
LEWIS RESEARCH CENTER
CLEVELAND, OHIO 44135

October 30, 1981

by

J. W. Kannel
and
J. L. Tevaarwerk (Consultant)

Battelle
Columbus Laboratories
505 King Avenue
Columbus, Ohio 43201

1. Report No.	2. Government Accession No.	3. Recipient's Catalog No.
NASA CR-165561		

4. Title and Subtitle	5. Report Date
Stress Evaluations Under Rolling/Sliding Contacts	October 30, 1981
	6. Performing Organization Code
7. Author(s)	8. Performing Organization Report No.
J. W. Kannel and J. L. Tevaarwerk	G7782
	10. Work Unit No.
9. Performing Organization Name and Address	
Battelle-Columbus Laboratories 505 King Avenue Columbus, Ohio 43201	11. Contract or Grant No. NAS 3-22808
	13. Type of Report and Period Covered Contractor's Report
12. Sponsoring Agency Name and Address	14. Sponsoring Agency Code

15. Supplementary Notes

Final Report. Project Manager, S. Loewenthal; Bearing, Gearing, and Transmission Section, NASA-Lewis Research Center, Cleveland, Ohio 44135.

16. Abstract

Computer models have been developed for analyzing the state-of-stress beneath traction-drive type of contacts. The analyses involve computing stresses and stress-reversals on various planes for points beneath the surface. The effect of tangential and axial friction under gross slip conditions can be evaluated with the models. Evaluations performed on an RC (rolling contact) tester configuration indicate that the classical fatigue stresses are not altered by friction-forces typical of lubricated contact. Higher values of friction ($f > 0.25$) can result in surface shear reversal that exceeds the stresses at the depth of maximum shear reversal under rolling contact.

17. Key Words (Suggested by Author(s))	18. Distribution Statement
Traction Drives, Traction Contacts, Reliability, Stress Analysis, Friction, Fatigue Life, Lubrication	Unclassified - Unlimited

19. Security Classif. (of this report)	20. Security Classif. (of this page)	21. No. of Pages	22. Price*
Unclassified	Unclassified	50	

* For sale by the National Technical Information Service, Springfield, Virginia 22161

NASA-C-168 (Rev. 10-75)

<u>TABLE OF CONTENTS</u>

<u>LIST OF FIGURES</u>

LIST OF FIGURES
(Continued)

LIST OF TABLES

ABSTRACT

Computer models have been developed for analyzing the state-of-stress beneath traction-drive type of contacts. The analyses involve computing stresses and stress-reversals on various planes for points beneath the surface. The effect of tangential and axial friction under gross slip conditions can be evaluated with the models. Evaluations performed on an RC (rolling contact) tester configuration indicate that the classical fatigue stresses are not altered by friction-forces typical of lubricated contact. Higher values of friction (f > 0.25) can result in surface shear reversal that exceeds the stresses at the depth of maximum shear reversal under rolling contact.

STRESS EVALUATIONS UNDER ROLLING/SLIDING CONTACTS

by

J. W. Kannel and J. L. Tevaarwerk (Consultant)

INTRODUCTION

Rolling elements such as roller bearings and traction drive transmissions are subject to failure from rolling contact fatigue. Such fatigue failures cause a serious restriction on the operating life and reliability of such devices. In the case of the traction drive transmissions, rolling contact fatigue failures could conceivably restrict the use of such transmissions in motor vehicles, despite the increased efficiency such transmissions could afford. Although a number of factors contribute to fatigue failure, the effect of traction and slip on the state of stress between rolling elements is not understood. A better understanding of the role of traction on fatigue could greatly assist in the evaluation of materials for and operational limits of traction components.

The fundamental theory for rolling contact fatigue is the one published by Lundberg and Palmgren(1)* in 1947 and summarized by Coy, et al.(2). This theory is based on the assumption that failure is in the form of shallow pitting and is related to subsurface shearing stresses within the rolling elements. In essence, any irregularity in the material beneath the surface can manifest itself as a failure initiation point. The significant stress field has been hypothesized as being bounded by the surface, the depth of the maximum and reversing shear stress, and the width of the rolling track. The magnitude and depth of the reversing shear stress have been found to be very significant with regards to fatigue failure.

The reversing stress field has been well established for pure rolling contacts(3,4). However, when surface tractions are imposed, this stress field becomes very complicated. The classic study for line contact is by Smith and Liu(5). Smith and Liu's research indicated that friction is a key

---

*References are listed at the end of the text.

factor with regards to reversing stresses. For example, at some level of friction, the reversing stress was found to be at the surface, which would greatly reduce fatigue life. Hamilton and Goodman(6) developed a theory for a circular sliding contact. The results of their theory are in the form of useful graphs for predicting friction effects for this specific type of contact. Other researchers, such as Kuznetsov(7), have studied the influence of friction on contact stress, but not on the subsurface stress field under slip conditions.

One complication to the reversing stress field is that the stress reversals occur over the width of contact and depend on orientation as well as depth. See, for example, Figure 1. The maximum stress occurs at the center of contact and the depth and magnitude are straightforward to compute. Computing the reversing stress becomes more complicated because the reversals occur over a finite region. Consider, then, the complication when the magnitude of τ_+ or τ_- depend on the orientation out of the plane of the paper.

The goal of the project has been to develop computer models to determine the magnitude of reversing shear stresses beneath (and very near) the surface of rolling/sliding contacts. Sliding in both the tangential direction and the axial direction are considered. Considerations are given for line contacts as well as crowned rollers. In order to insure accuracy in modeling, two independent models were developed, one by Tevaarwerk (T-model) and one at Battelle (B-model)*. This approach allowed for both researchers to be heavily involved with the problem in modeling and created excellent dialogue, both for the mathematical intricacies, as well as the ramification of the predictions. A comparison between the two models is given in Table 1, which demonstrates the consistency of the two approaches. The approach for the development of the models was as follows:

- Define the stress tensor for any point beneath the surface
- Compute principal stresses and their direction cosines for each point
- Determine the direction cosines (relative to the x, y, z axes) to the octahedral plane and the plane of maximum shearing stress

---

*As discussed in Appendix A, the primary difference in the two models is in the integration scheme used to determine the stress tensor.

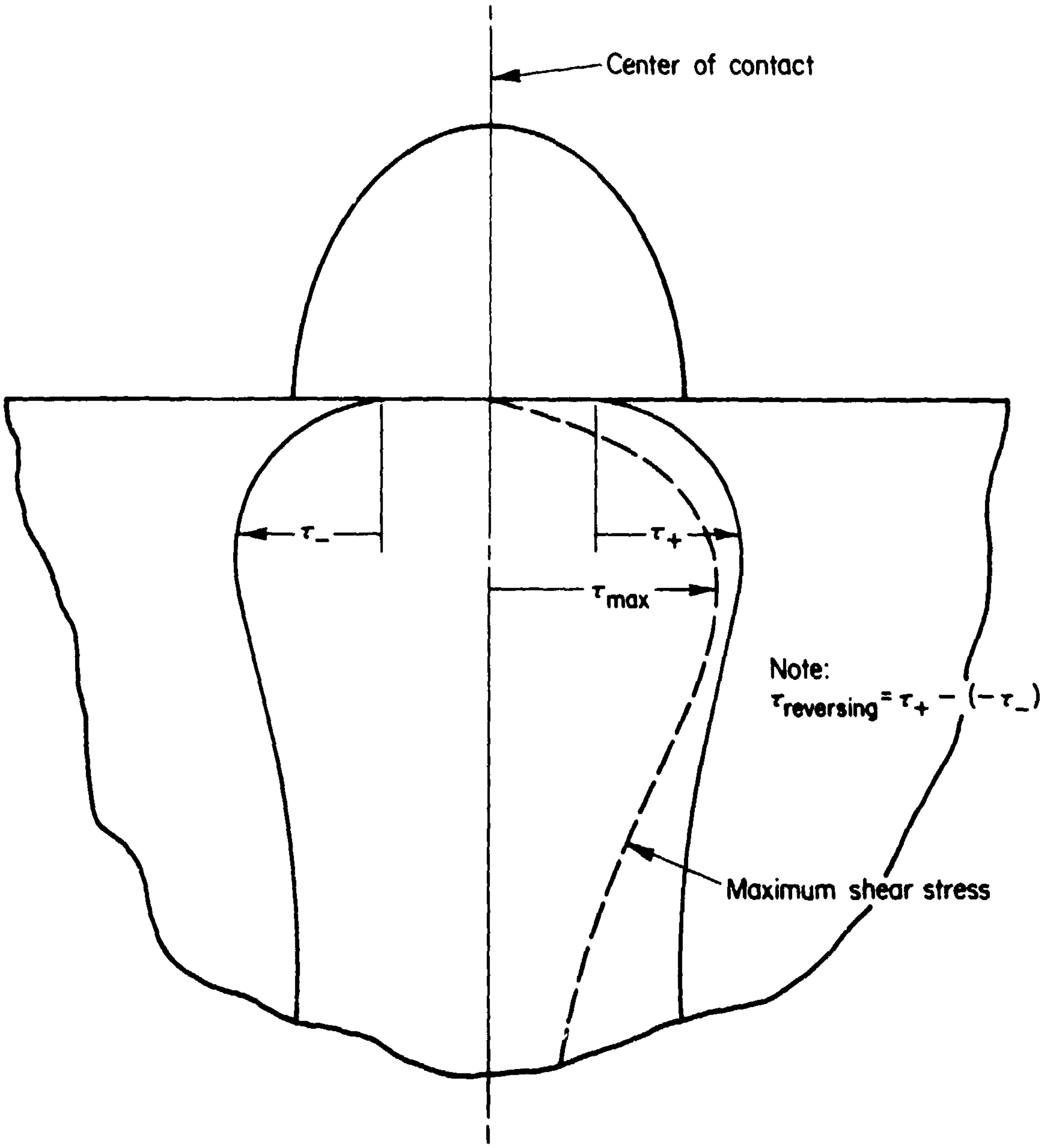

FIGURE 1. ILLUSTRATION OF SHEAR STRESS BENEATH THE SURFACE OF CONTACT

TABLE 1. COMPARISON OF TEVAARWERK MODEL WITH BATTELLE MODEL
($K = .5$, $\nu = .285$, $f_A = 0$, $z/b = .3$)

f_T	z/b	σ_x T	σ_x B	σ_y T	σ_y B	σ_z T	σ_z B	τ_{xy} T	τ_{xy} B	τ_{yz} T	τ_{yz} B	τ_{xz} T	τ_{xz} B
0	-.9	-.236	-.241	-.212	-.218	-.375	-.383	0	0	0	0	.228	.231
	-.8	-.251	-.256	-.255	-.259	-.511	-.518	0	0	0	0	.222	.225
	-.5	-.329	-.333	-.361	-.369	-.798	-.807	0	0	0	0	.138	.140
	-.3	-.374	-.380	-.404	-.412	-.896	-.907	0	0	0	0	.080	.081
	0	-.401	-.408	-.428	-.436	-.948	-.958	0	0	0	0	0	0
	.3	-.374	-.380	-.404	-.412	-.896	-.907	0	0	0	0	-.080	-.081
	.5	-.329	-.333	-.361	-.369	-.798	-.807	0	0	0	0	-.138	-.141
	.8	-.251	-.256	-.255	-.259	-.511	-.518	0	0	0	0	-.222	-.225
	.9	-.236	-.240	-.212	-.218	-.375	-.383	0	0	0	0	-.228	-.230
.1	-.9	-.171	-.174	-.196	-.201	-.352	-.360	0	0	0	0	.195	.200
	-.8	-.188	-.191	-.239	-.243	-.489	-.495	0	0	0	0	.187	.190
	-.5	-.281	-.284	-.349	-.356	-.784	-.793	0	0	0	0	.095	.097
	-.3	-.344	-.349	-.396	-.414	-.888	-.898	0	0	0	0	.032	.033
	0	-.401	-.408	-.428	-.436	-.948	-.958	0	0	0	0	-.051	-.051
	.3	-.404	-.411	-.412	-.420	-.904	-.915	0	0	0	0	-.128	-.130
	.5	-.376	-.382	-.373	-.381	-.812	-.821	0	0	0	0	-.182	-.184
	.8	-.315	-.320	-.271	-.276	-.533	-.540	0	0	0	0	-.256	-.260
	.9	-.301	-.308	-.228	-.234	-.398	-.406	0	0	0	0	-.260	-.264

- Scan the planes of octahedral and maximum shearing stress in the direction of rolling and compute stress reversals.

Stress reversals can be computed by the above procedure for conditions of zero friction, axial friction, and tangential friction for line contacts and contacts corresponding to a rolling contact fatigue tester. The basic assumptions for the analyses are:

1. The contact pressure (normal stress) are predictable by Hertz theory for line or crowned contacts.
2. The contact tractions are a result of a constant traction coefficient times the pressure. This tacitly assumes a gross sliding situation.
3. The materials are all elastic and homogeneous.
4. The bodies are isothermal. That is, no thermal stresses are considered.

MODEL DEVELOPMENT

The Stress Tensor

The objective of the analyses is to evaluate subsurface stresses in rolling/sliding contacts of the type seen in traction drives. Consider, for example, the system shown in Figure 2, where two cylinders are loaded together under rolling or possibly rolling/sliding contact. The assumed Hertzian contact pressure distribution produces a state of stress throughout the cylinders. Likewise, the frictional forces associated with sliding produce an additional state of stress such that a typical point beneath the surface is undergoing a complicated and changing stress state. For crowned cylinders, this stress state varies axially (in the y direction) as a result of axially varying pressures as well as in the x direction, as shown in Figure 3.

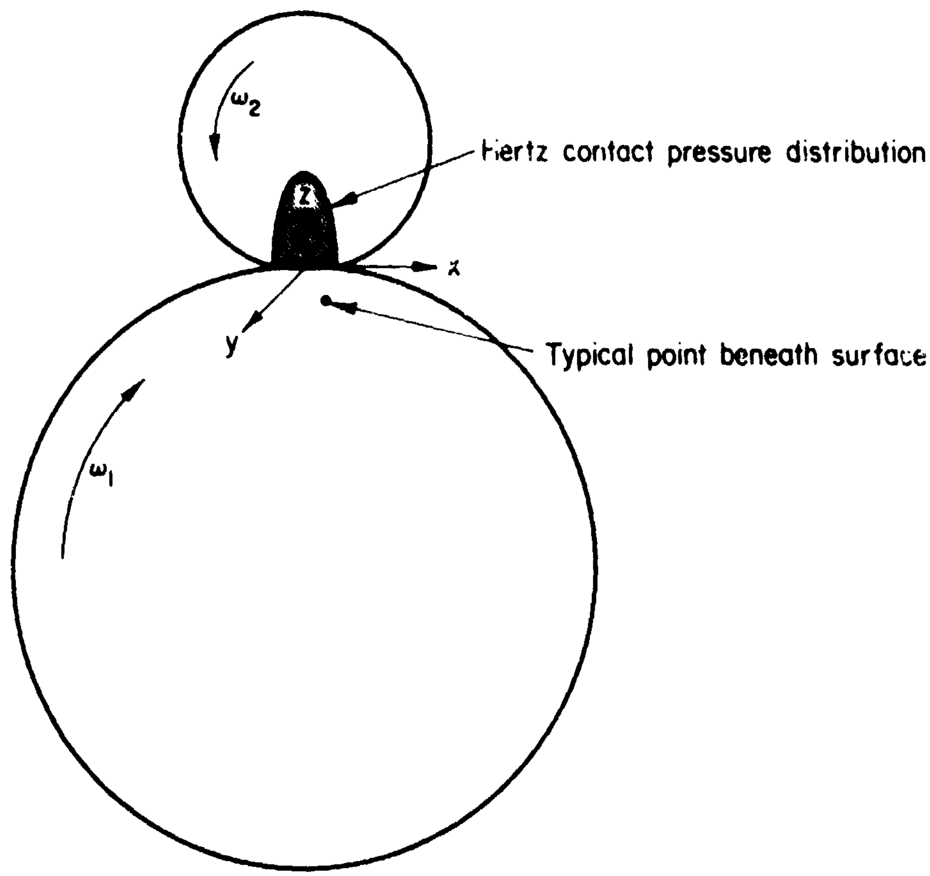

FIGURE 2. CONTACT BETWEEN ROLLING/SLIDING BODIES

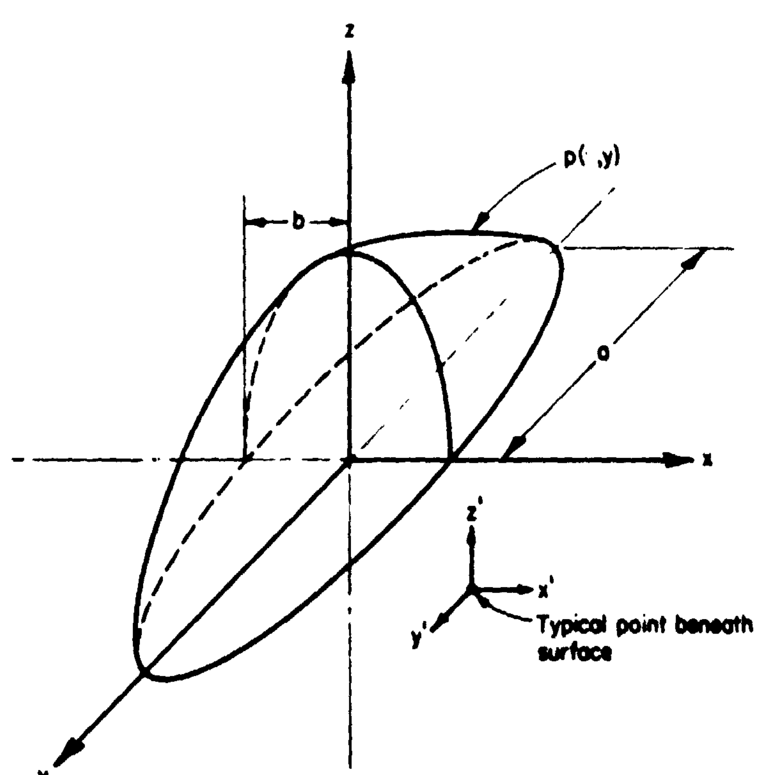

FIGURE 3. PRESSURE ELLIPSE

In tensor notation, the stress at any point can be written as

$$\sigma_{ij} \quad \text{or} \quad \overline{\sigma}_{ij} \quad , \tag{1}$$

where $\quad \overline{\sigma}_{ij} = \sigma_{ij}/p_H \qquad (i, j = 1, 2, 3) \quad ,$

where p_H is the maximum Hertz contact pressure. In more conventional terminology

$$\begin{aligned} \sigma_x = \sigma_{11} \ , \quad \sigma_y = \sigma_{22} \quad , \quad \sigma_z = \sigma_{33} \quad , \\ \tau_{xy} = \sigma_{12} \ , \ \tau_{xz} = \sigma_{13} \text{ and } \tau_{yz} = \sigma_{23} \quad . \end{aligned} \tag{2}$$

It should be noted that the stress tensor is symmetric such that $\sigma_{ij} = \sigma_{ji}$.

To determine σ_{ij} requires that expressions be developed for the effect of point loads on stresses and that the point loads be integrated over the conditions of interest. These equations are discussed in Appendix A and Equation A-27 shows the general relationship for $\overline{\sigma}_{ij}$ of interest here.

Principal Stresses

From the preceding discussions, it can be noted that the state of stress at any point has six components*. The components discussed in the preceding section describe the stress when the axis is oriented in the x, y, z system. However, the stress can look considerably different at different orientations. Since the objective of the study is to evaluate "worse case" shear stresses, it is necessary to evaluate the effect of axis rotation (see Figure 4) on stress. The first step in this phase of the study is to determine the parameters that are not a function of rotation; these are known as the invariants of the stress tensor[8]. These invariants are:

---

*Actually nine components are required, but some are equal because of symmetry.

$$I_r = \sigma_{11} + \sigma_{22} + \sigma_{33} \quad , \tag{3}$$

$$II_r = \sigma_{11}\,\sigma_{22} + \sigma_{11}\,\sigma_{33} + \sigma_{22}\,\sigma_{33} - \sigma_{12}^2 - \sigma_{13}^2 - \sigma_{23}^2 \quad \text{, and} \tag{4}$$

$$III_r = \sigma_{11}\,\sigma_{22}\,\sigma_{33} + 2\sigma_{12}\,\sigma_{23}\,\sigma_{13} - \sigma_{11}\,\sigma_{23}^2 - \sigma_{22}\sigma_{13}^2 - \sigma_{33}\sigma_{12}^2 \quad . \tag{5}$$

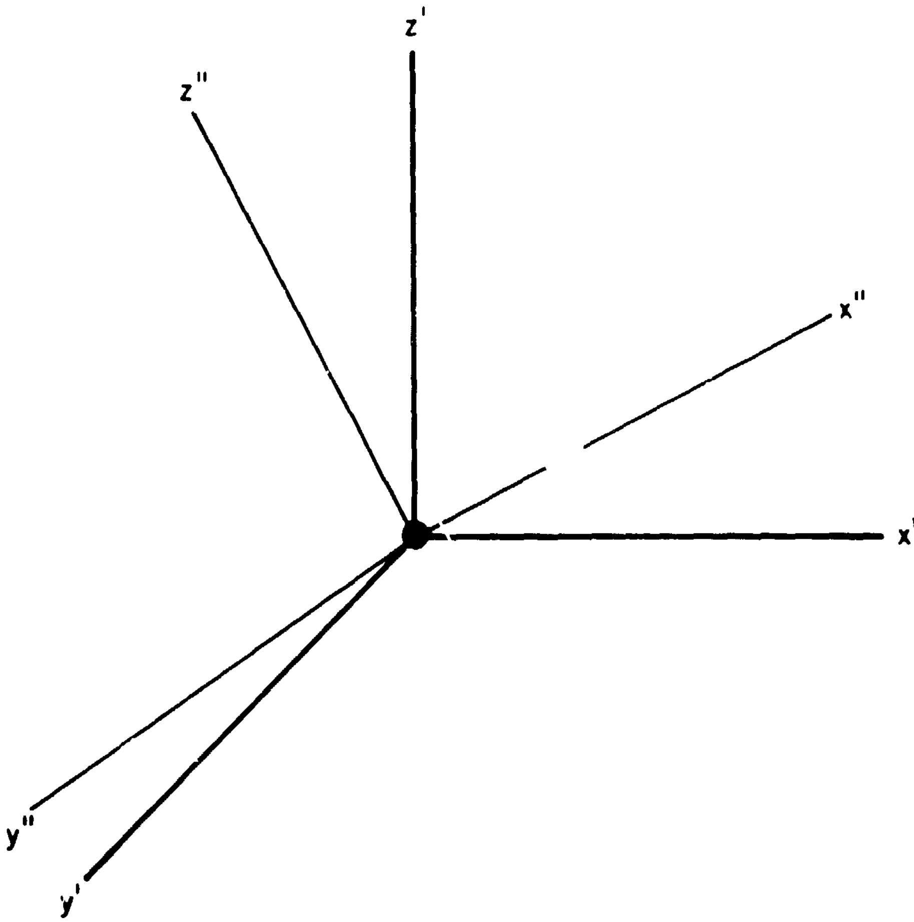

FIGURE 4. ILLUSTRATION OF AXIS ROTATION

With the knowledge of the invariants, it is possible to determine the plane of the principal stress (i.e., the rotated axis on which no shear forces exist) and the stress magnitudes. The equations for the principal stresses can be written

$$S^3 + I_r S^2 + II_r S + III_r = 0 \quad . \tag{6}$$

Equation 6 can be readily solved by cubic equation solutions and will produce three real roots for principal stresses. These roots will be known as S_1, S_2, and S_3 with S_1 being the largest and S_3 the smallest.

Angles To The Principal Stresses

In tensor computations, the angles are given in terms of direction cosines to the various axes. If we define a_{nx}, a_{ny}, and a_{nz} as the direction cosines from a given principal stress (say S_1) to the x, y, and z axis, then it can be shown that the following equations must be satisfied(8):

$$a_{nx1}{}^2 + a_{ny1}{}^2 + a_{nx1}{}^2 = 1 \quad , \tag{7}$$

$$(\sigma_{11} - S_1)\, a_{nx1} + \sigma_{12}\, a_{ny1} + \sigma_{13}\, a_{nz1} = 0 \quad , \tag{8}$$

$$\sigma_{12} a_{nx1} + (\sigma_{22} - S_1)\, a_{ny1} + \sigma_{23}\, a_{nz1} = 0 \quad \text{, and} \tag{9}$$

$$\sigma_{13}\, a_{nx1} + \sigma_{23}\, a_{ny1} + (\sigma_{33} - S_1)\, a_{nz1} = 0 \quad . \tag{10}$$

By solving Equation 7 and any two of Equations 8 through 10 simultaneously, a_{nx1}, a_{ny1} and a_{nz1} can be determined. In a like manner, the direction cosines for locating the S_2 (a_{nx2}, a_{nz2}, a_{nz2}) and the S_3 (a_{nx3}, a_{ny3}, a_{nz3}) stress can be determined.

Other Planes of Interest

The solution of equation 7 through 10 permit the determination of the location of principal stresses. However, the objective of the project is to evaluate shear stresses and by definition there are no shear stresses on these planes. Therefore, other planes must be considered.

Plane of Maximum Shear Stress

The maximum shear stress for an element lies on a plane bisecting the $S_1 - S_3$ plane. The direction cosines for the normal to this plane relative to the plane of the principal stress axes can be written

$$b_{n1} = 1/\sqrt{2} \quad , \tag{11}$$

$$b_{n2} = 0. \quad , \tag{12}$$

$$b_{n3} = 1/\sqrt{2} \quad . \tag{13}$$

To relate these cosines back to the x, y, z axis requires an angle transformation of the form

$$c_{nx} = b_{n1}\ a_{nx1} + b_{n2}\ a_{nx2} + b_{n3}\ a_{nx3} \quad , \tag{14}$$

$$c_{ny} = b_{n1}\ a_{ny1} + b_{n2}\ a_{ny2} + b_{n3}\ a_{ny3} \quad , \tag{15}$$

$$c_{nz} = b_{n1}\ a_{nz1} + b_{n2}\ a_{nz2} + b_{n3}\ a_{nz3} \quad , \tag{16}$$

where c_{n1}, c_{n2} and c_{n3} are the direction cosines from the normal (to the shear plane) to the x, y, z axes.

Plane of Octahedral Stress

The location of the normal to the octahedral stress can be written

$$b_{n1} = 1/\sqrt{3} \quad , \tag{17}$$

$$b_{n2} = 1/\sqrt{3} \quad , \tag{18}$$

$$b_{n3} = 1/\sqrt{3} \quad . \tag{19}$$

That is, the normal is situated at equal angles from the principal axis. Likewise, Equations 17 through 19 can be used in conjunction with Equations 14 through 16 to relate the normal to the x, y, z axes.

Seeking The Maximum and Minimum Shear Stresses

Using the angle transformation equations discussed in the previous section, it is possible to locate the normals to various critical shear stress planes. The final step in this process is to locate maximum and minimum shear stress on those particular planes for various x positions. Let us define the direction cosines to a given location on a shear plane as a_{sx}, a_{sy} and a_{sz}. It can be shown that[8]

$$a_{sx}\, c_{nx} + a_{sy}\, c_{ny} + a_{sz}\, c_{nz} = 0 \quad \text{and} \tag{20}$$

$$a_{sx}^2 + a_{sy}^2 + a_{sz}^2 = 1 \quad . \tag{21}$$

If, then, we choose a particular angle, say a_{sx}, we can compute a_{sy} and a_{sz} by Equations 20 and 21.

With a knowledge of the angles between the shear vector on a plane and the x, y, z axes and a knowledge of the stress tensor as oriented to the x, y, z axes, the shear stress can be computed. The equation for the stress is given by[8]

$$\begin{aligned} \tau = {} & c_{nx}\, a_{sx}\, \sigma_{11} + c_{ny}\, a_{sy}\, \sigma_{22} + c_{nz}\, a_{sz}\, \sigma \quad , \\ & + c_{nx}\, a_{sy}\, \sigma_{12} + c_{ny}\, a_{sx}\, \sigma_{12} + c_{nx}\, a_{sz}\, \sigma_{13} \quad , \\ & + c_{nz}\, a_{sx}\, \sigma_{13} + c_{ny}\, a_{sz}\, \sigma_{23} + c_{nz}\, a_{sy}\, \sigma_{23} \quad . \end{aligned} \tag{22}$$

In the computer model, values of a_{sx} were assumed in the range -1 to +1. For each value of a_{sx}, the shear stress was computed at various x positions and both the maximum and minimum values were stored. In the computation, the maximum shear stress and the maximum reversal $\tau_{max} - \tau_{min}$ were sought.

Construction Of Model

The computer model is constructed as follows:

1. Input values of κ (b/a), ν (Poissons ratio), z/b (depth) f_T (tangential friction coefficient), f_A (axial friction coefficient), and case number.
2. Compute the stress tensor for approximately eleven (11) x locations (STRSSC). For K = 0 (line contact), the Smith-Liu[5] solutions are used.
3. Compute the principal stresses at each x location (PRINC).
4. Compute the angles to the principal stresses at each location (ANGLP).
5. Compute the angle to the normals of the maximum shear plane, the octahedral shear plane, and the orthogonal plane (ANGTRAN).
6. Compute the shear stresses and shear reversals on the shear planes (RVSTRS).

All computations are in the form σ_{ij}/p_H and are applicable for any (elastic) contact pressure level. A source listing for the model is given in Appendix B and a typical printout is given in Table 2.

In this table

K = b/a (aspect ratio)

NU = (Poissons ratio)

Z = z/b (depth into surface)

F_T = f_T (tangential friction coefficient)

F_A = f_A (axial friction coefficient)

S_{XX}, S_{YY}, S_{ZZ} are the normal stresses (σ_x, σ_y, σ_z)

S_{XY}, S_{YZ}, S_{XZ} are the shear stress (τ_{xy}, τ_{yz}, τ_{xz})

S_1, S_2, S_3 are the principal stresses

X - pos = x/b is the x position being evaluated

TAU-MAX = maximum shearing stress as computed by scanning different planes

AN (1), AN (2), AN (3) are the direction cosines to the normals on the planes containing TAU-MAX and, AS (1), AS (2), AS (3) are the direction cosines to TAU-MAX on the shear plane.

TABLE 2. TYPICAL PRINTOUT FOR BATTELLE STRESS MODEL

CASE NUMBER= 100

K= .80000E+00 NU= .28500E+00 Z= .10000E+00 FT= .10000E+00 FA= 0.

IX	SXX	SYY	SZZ	SXY	SYZ	SXZ	S1	S2	S3	X-POS
1	-.59283E-01	-.17261E+00	-.13866E+00	.35355E-08	.35355E-08	.11783E+00	.25361E-01	-.17262E+00	-.22331E+00	-.10000E+01
2	-.11560E+00	-.26274E+00	-.39002E+00	.3521 -08	.35213E-08	.11627E+00	-.72964E-01	-.26274E+00	-.43265E+00	-.90000E+00
3	-.21121E+00	-.34511E+00	-.56935E+00	.35295E-08	.35295E-08	.77424E-01	-.19519E+00	-.34511E+00	-.58538E+00	-.80000E+00
4	-.45779E+00	-.51183E+00	-.85826E+00	.35244E-08	.35244E-08	-.10770E-01	-.45750E+00	-.51183E+00	-.85855E+00	-.50000E+00
5	-.56596E+00	-.57347E+00	-.95228E+00	.35446E-08	.35446E-08	-.45295E-01	-.56072E+00	-.57347E+00	-.95752E+00	-.30000E+00
6	-.65376E+00	-.61313E+00	-.10029E+01	.35196E-08	.35196E-08	-.81005E-01	-.61313E+00	-.63588E+00	-.10208E+01	0.
7	-.65600E+00	-.59489E+00	-.95857E+00	.35446E-08	.35446E-08	-.10808E+00	-.59489E+00	-.62136E+00	-.99321E+00	.30000E+00
8	-.60578E+00	-.54672E+00	-.86971E+00	.35244E-08	.35244E-08	-.12563E+00	-.54672E+00	-.55554E+00	-.91995E+00	.50000E+00
9	-.42607E+00	-.39441E+00	-.59386E+00	.35295E-09	.35295E-08	-.16825E+00	-.32196E+00	-.39441E+00	-.69797E+00	.80000E+00
10	-.33809E+00	-.31191E+00	-.41976E+00	.35213E-08	.35213E-08	-.18799E+00	-.18655E+00	-.31191E+00	-.57129E+00	.90000E+00
11	-.26966E+00	-.21612E+00	-.16702E+00	.35355E-08	.35355E-08	-.17406E+00	-.36877E-01	-.21612E+00	-.39981E+00	.10000E+01

FATIGUE SHEAR STRESS SUMMARY

PLANE OF MAX SHEAR STRESS

TAU MAX= .20372E+00 AN(1)= -.21583E+00 AN(2)= .70711E+00 AN(3)= -.67337E+00 X-REF= .30000E+00
TAU REVERSING= .32192E+00 AS(1)= -.10000E+00 AS(2)= -.70200E+00AS(3)= -.70512E+00

PLANE OF MAX OCT SHEAR STRESS

TAU MAX= .20014E+00 AN(1)= -.18715E+00 AN(2)= .57735E+00 AN(3)= .79476E+00 X-REF= .80000E+00
TAU REVERSING= .27615E+00 AS(1)= -.50000E+00 AS(2)= .64042E+00AS(3)= -.58297E+00

PLANE OF REVERSING SHEAR STRESS

TAU MAX= .18799E+00 AN(1)= 0. AN(2)= 0. AN(3)= .10000E+01 ·REF=
TAU REVERSING= .30582E+00 AS(1)= -.10000E+01 AS(2)= 0. AS(3)= 0.

TAU-REVERSING is the maximum reversing shear stress on the planes specified.

ANALYSIS FOR RC FATIGUE TESTER

One objective of the project has been to evaluate the effect of magnitude and direction of slip on the stresses in a rolling contact (RC) fatigue tester. The RC tester consists of a rotating cylindrical specimen loaded between two large diameter crowned rollers. In the test, the specimen is driven by an electric motor; the crowned rollers are only driven by the specimen. The rollers are loaded to a level to produce fatigue in the specimen in a reasonable time period. Normally, the RC tester is used to evaluate rolling contact fatigue and has been used in bearing-material evaluations. The tester is also being considered as a candidate device for evaluating the effect of friction on fatigue.

Two approaches could be used to induce friction between the cylindrical specimen and the crowned rollers. One technique would be to induce a drag between the two elements by driving or braking the rollers. This approach could be quite complicated for simple fatigue testing and an alternate could be more desirable. This alternate approach could consist simply of skewing the specimen relative to the rollers. However, skewing produces an axial traction, whereas braking the rollers produces a tangential traction. The stress model can be used in determining the stress fields associated with these two types of fatigue test concepts.

Typical dimensions for an RC rig are

D_s = 9.5 mm (0.375 inch)

D_r = 190 mm (7.5 inches)

R_c = 6.4 mm (0.25 inch).

D_s is the specimen diameter, D_r is the roller diameter, and R_c is the crown radius. For these dimensions, a value of $K = 0.8$ has been computed. The upper limit traction coefficient should be nominally 0.1 for lubricated tractions.

Figure 5 shows the effect of traction on the reversing shear stresses in the RC tester. As can be observed, the maximum stress is unaffected by the

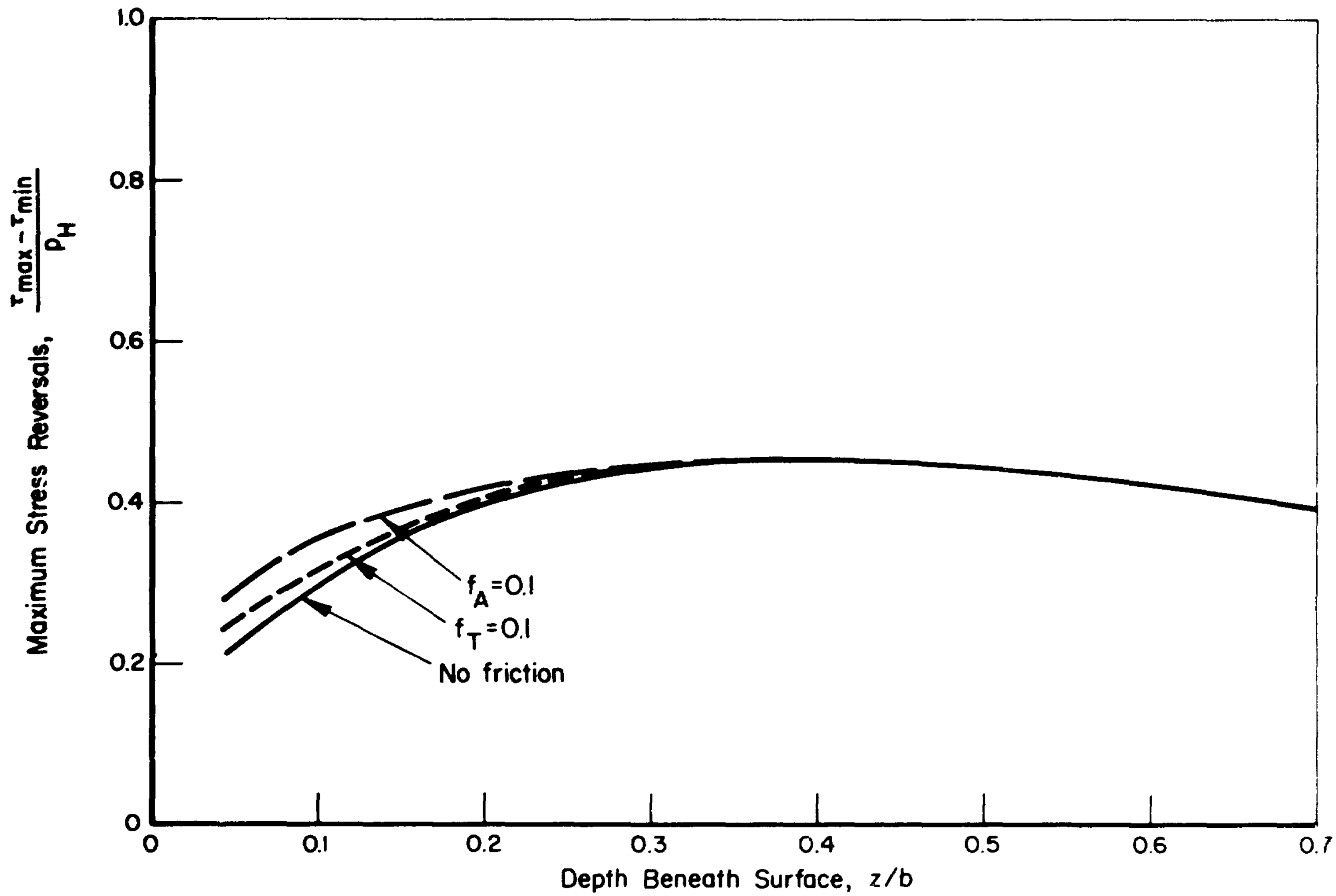

FIGURE 5. EFFECT OF FRICTION ON REVERSING SHEAR STRESS FOR RC TESTER (K = .8, ν = .285, B-Model)

friction as is the depth to maximum stress ($z/b = 0.38$). There are some differences in the stresses near the surface, and it is impossible to be certain how these differences affect life. However, in the Lundberg-Palmgren theory, only the orthogonal shear reversal and its depth are important. If this theory is valid, it says that a traction coefficient of up to 0.1 should not alter life. There is, however, a difference in off-set between axial and tangential-friction, but this effect is not a part of fatigue theory. Fatigue tests are badly needed to clarify the effect of stress on life.

The general observation from this aspect of the analyses is that the direction of the traction is not significant with regards to fatigue type stress for low traction coefficients typical of lubricated contacts assuming Lundberg-Palmgren's theory. It should be noted that at least three stress related factors that have not been included in these stress analyses could have a profound effect on fatigue. These factors are:

(1) the effect of temperature (due to friction) on stress

(2) the effect of non-Hertzian pressure on stress

(3) the effect of asymmetric surface traction.

All of these can produce an asymmetry in stresses which can amplify the stress reversal. In fact, there will be a different stress state in the driver and driven for effects (1) and (3). The influence of the non-Hertzian pressure should be the same on both bodies provided that we do not invoke hysteresis effects in the material.

If we examine the influence of (1) and (3) on, say, the reversing orthogonal stress and assume that the traction is caused by the shearing of an elastic/plastic-like material, then the surface traction in the latter half of the contact is larger than in the front. Also the traction stresses will be negative in direction on the driver and positive on the driven. This means that the stress reversal in the driven is increased from the non-traction condition while it is decreased in the driver, possibly explaining some of the experimental findings reported elsewhere. The depth at which the maximum orthogonal acts is also reduced by an asymmetric traction stress. Traction produced by an elastic/plastic-like material may also explain why gears fail by pitting fatigue in the region directly below the pitch circle because the positive sliding conditions may produce a region of maximum surface traction asymmetry and, hence, the largest magnitude of the reversing orthogonal shear stress. The thermal stresses produced by the sliding would also alter the stress profile for the orthogonal shear stress in a similar fashion but now because the driver (i.e., the faster moving body) would see a lower flash temperature than the driven. Thermal stresses would tend to increase the orthogonal shear stress in b·th bodies but more in the driven than the driver. Also besides the increases in the amplitude of the stress reversal, the depth at which this occurs is reduced, giving a further reduction in fatigue life on the driver. Further research is needed in this area to establish the influence of the effects just mentioned.

DISCUSSION OF EFFECTS OF FRICTION ON FATIGUE STRESSES

The subsurface stress model represents a useful tool for evaluating the role of friction on fatigue type stresses. The results of the evaluations of the stress analyses from the RC tester showed some interesting (although perhaps not profound) implications of the effect of lubricated traction on stresses. The purpose of this section is to further explore the effect of friction on stress.

Figures 6 through 8 show predictions of the reversing orthogonal shear stress for various conditions of friction and aspect ratio (b/a). This reversing stress is normally considered the significant stress for fatigue.(1) Note, however, in Figure 6, that friction does not alter the magnitude of the difference between maximum and minimum shear stress (i.e., stress reversals). This implies that the magnitude of the orthogonal stress reversals are not dependent on friction. Changing aspect ratio does alter the magnitude of the stress as shown in Figures 9 and 10, but this dependence of stress on aspect ratio is not affected by friction.

The effects of friction on the magnitude and depth of the maximum shear stress, are shown in Figures 11 and 12 for various values of aspect ratio. Some increase in stress accompanies an increase in friction. However, for $f_T = .1$ and $\nu = .285$ which are reasonable values for lubricated traction

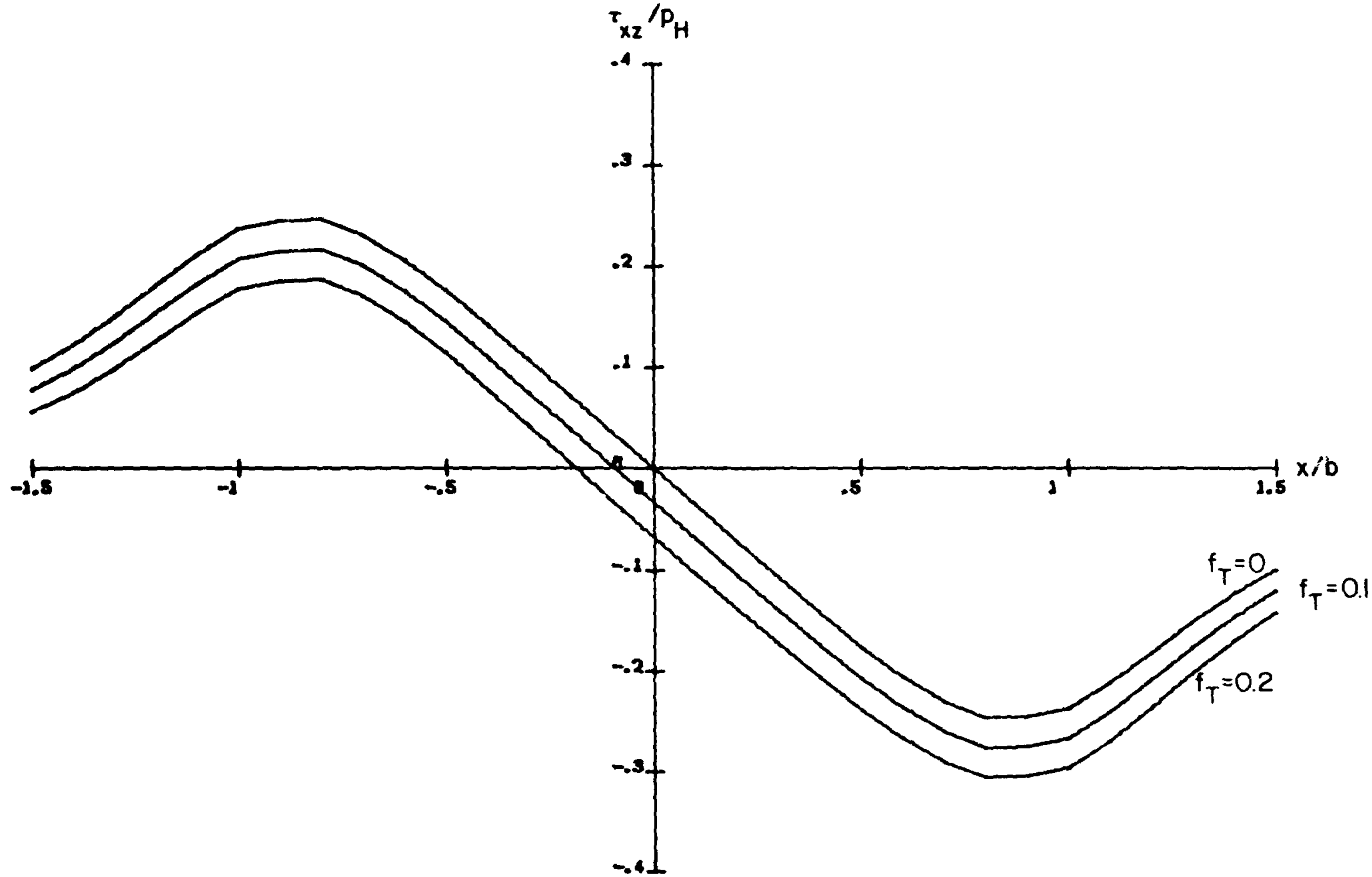

FIGURE 6. EFFECT OF FRICTION ON REVERSING ORTHOGONAL SHEAR STRESS
(K = 0, ν = .285, z/b = .5 T-Model)

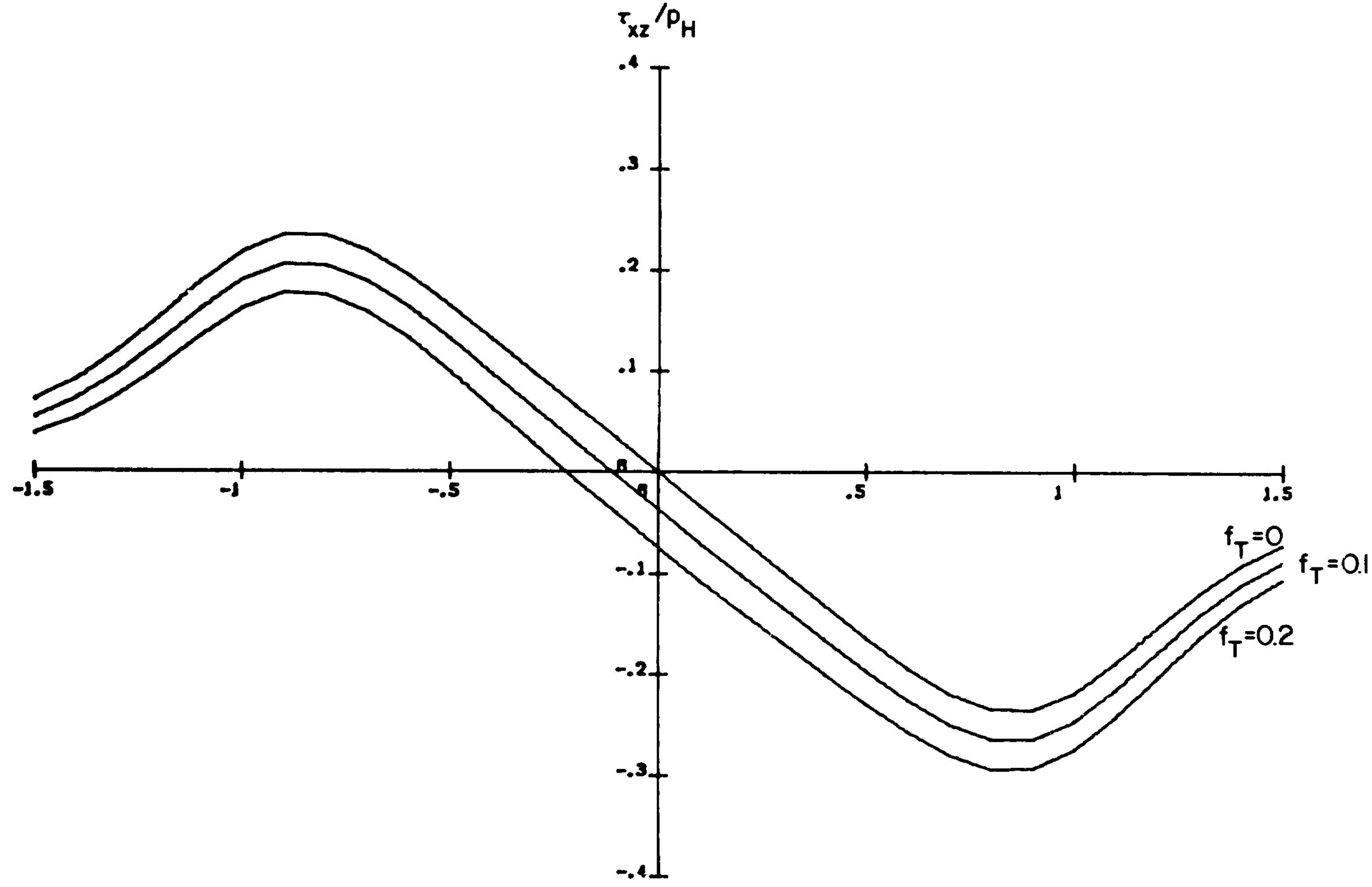

FIGURE 7. EFFECT OF FRICTION ON REVERSING ORTHOGONAL SHEAR STRESS
(K = .5, ν = .285, z/b = .435 T-Model)

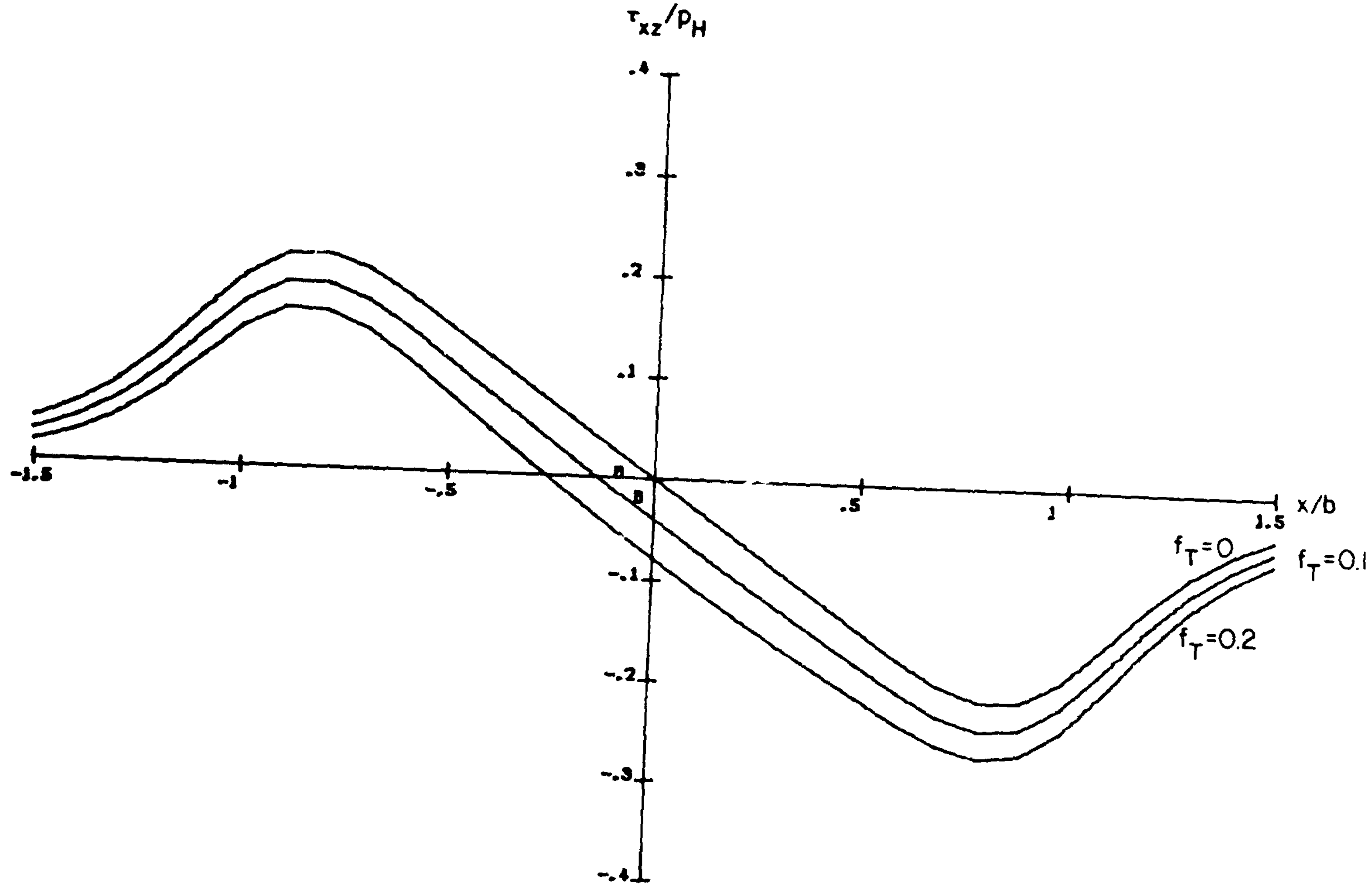

FIGURE 8. EFFECT OF FRICTION ON REVERSING ORTHOGONAL SHEAR STRESS
(K = 1, ν = .285, z/b = .35 T-Model)

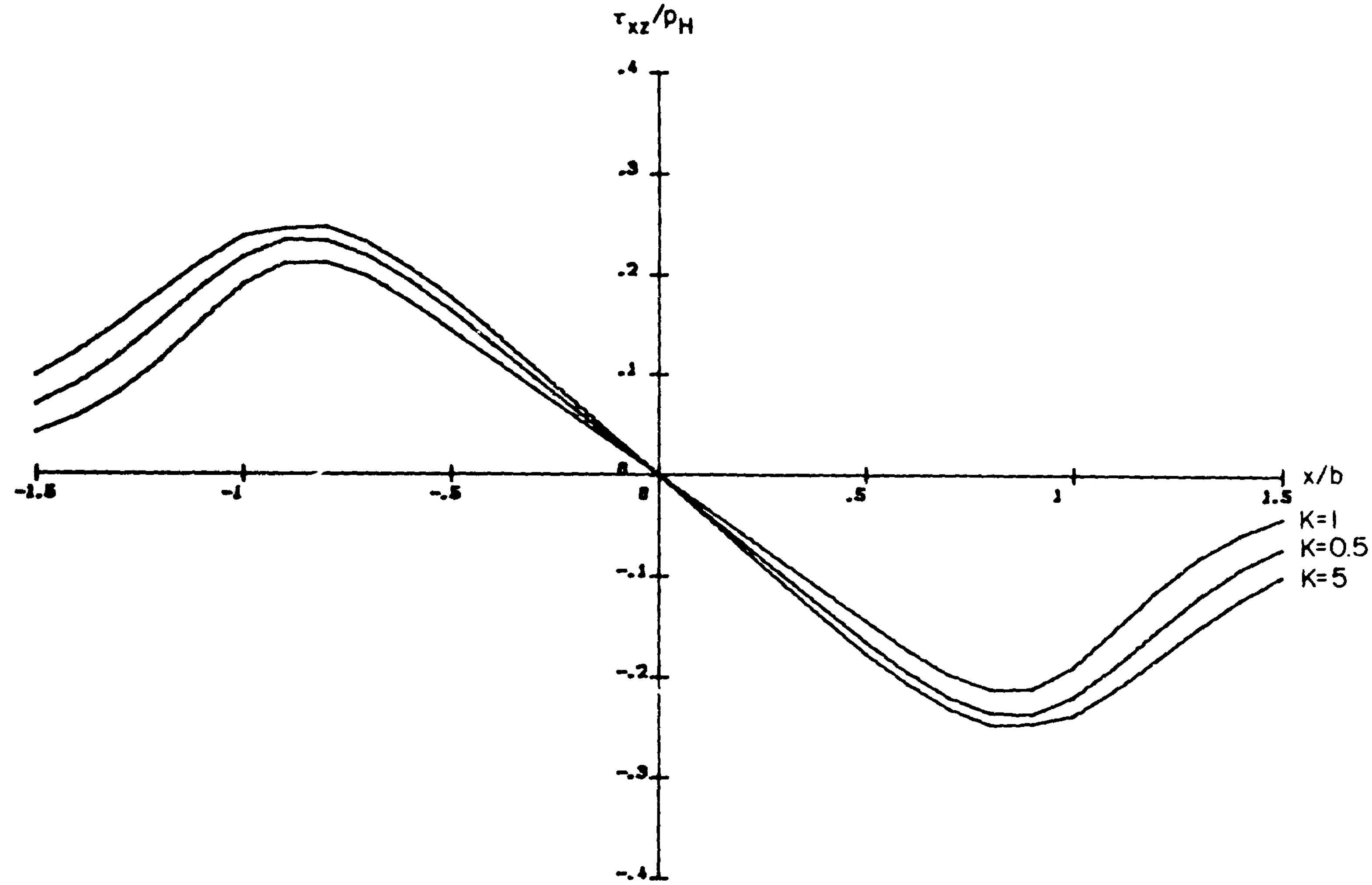

FIGURE 9. EFFECT OF ASPECT RATIO K ON REVERSING ORTHOGONAL SHEAR STRESS ($f_T = f_A = 0$, $\nu = .285$ T-Model)

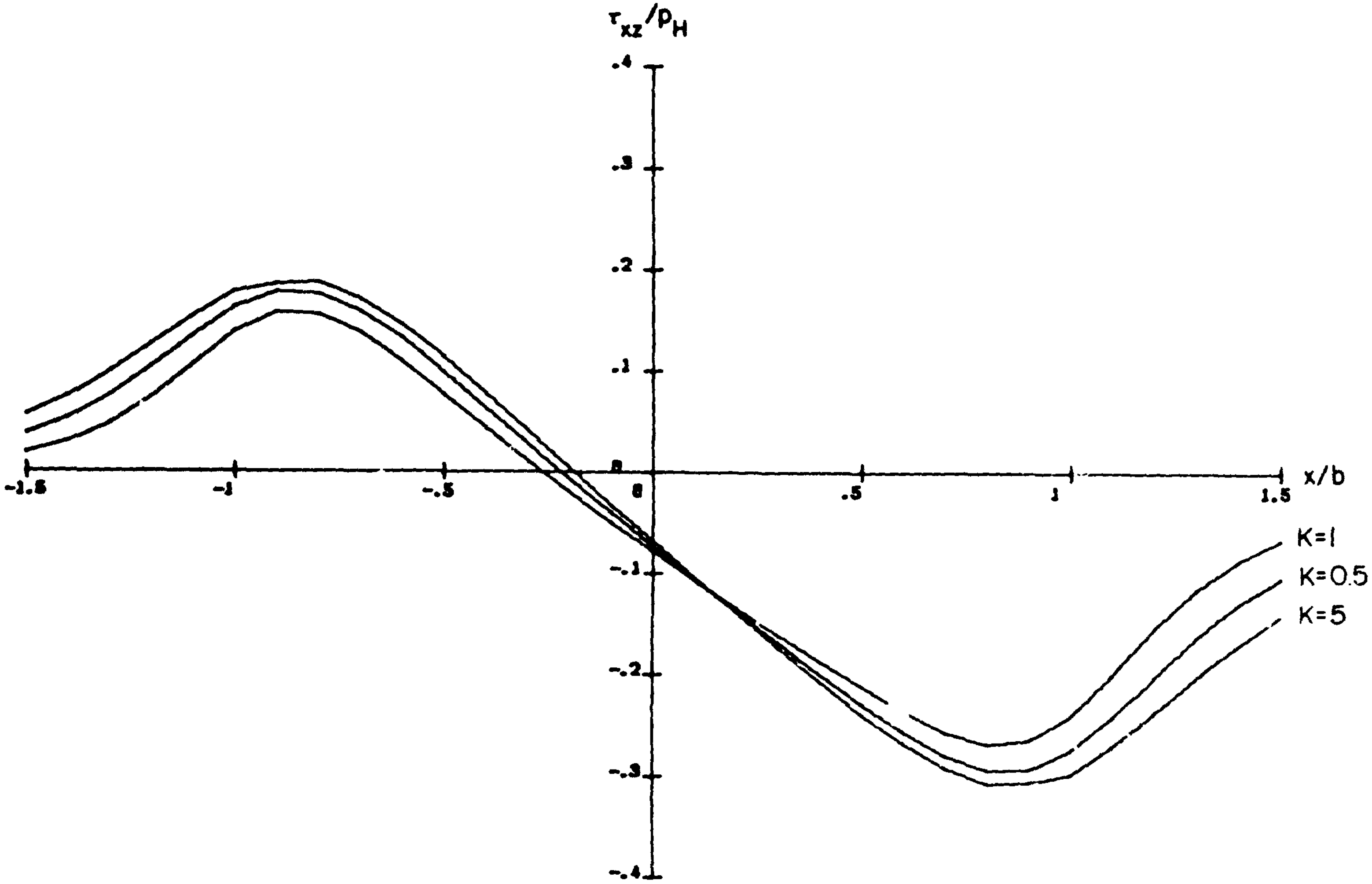

FIGURE 10. EFFECT OF ASPECT RATIO ON REVERSING ORTHOGONAL SHEAR STRESS
(f_r = .2, ν = .285 T-Model)

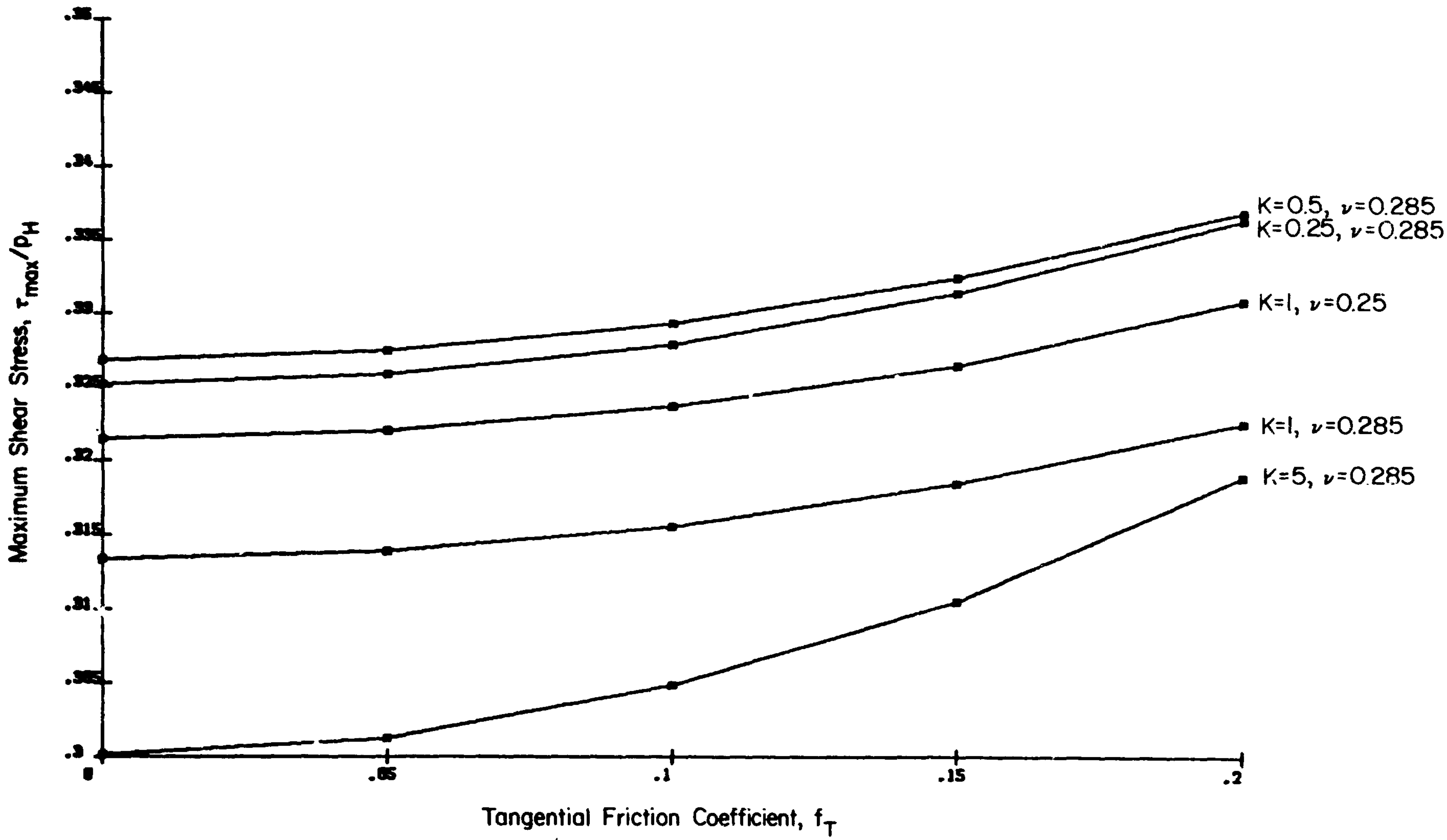

FIGURE 11. EFFECT OF FRICTION ON MAGNITUDE OF MAXIMUM SHEAR STRESS (T-Model)

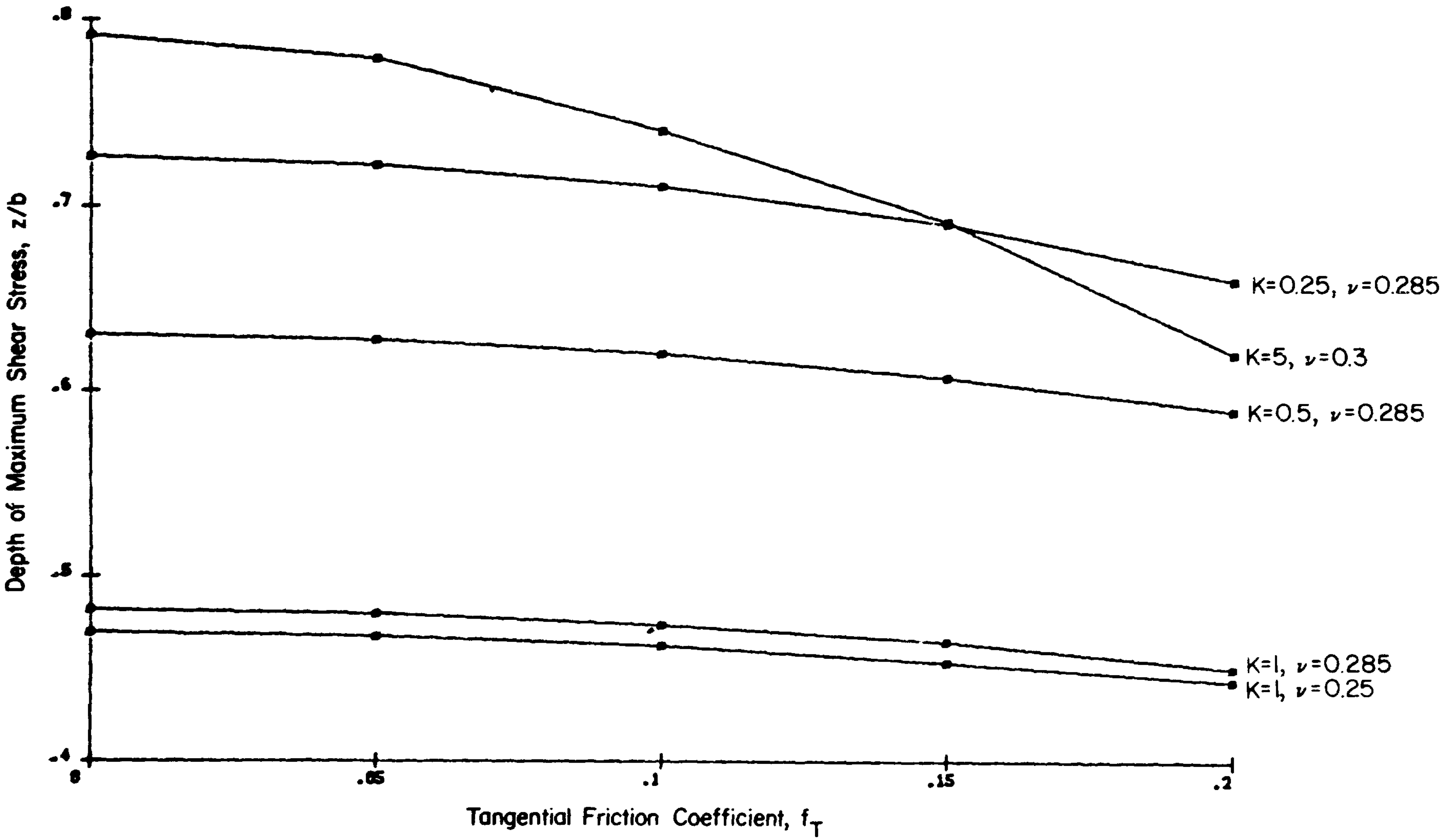

FIGURE 12. EFFECT OF FRICTION ON DEPTH OF MAXIMUM SHEAR STRESS (T-Model)

drives, only very small changes in stress depth and magnitude occur. Higher value of friction (f = .2) produces sizable increases in stress. The observations concerning shear stress also occur with regard to the octahedral shear stress as shown in Figures 13 and 14.

Figure 15 shows the effect of friction coefficient, f, on surface-shear-stresses-reversals for line (K = 0) contact. As can be observed, the magnitude of reversing stresses on the surface does not exceed the reversing orthogonal shear stress for values of f < 0.25. This implies that for this contact situation, fatigue-related stresses are not altered by friction for f < 0.25. Smith and Liu[5] showed sizable effects at f = 0.33, which would be consistent with our computations. However, values of f of this magnitude should occur only in very poor lubrication situations and are not relevant to lubricated traction drive theory. As can be observed, friction does materially alter the shear stresses near the surfaces, even for low (< 0.1) friction coefficients. This implies that friction alters the overall stress field and could alter the propensity of the system to incur a surface or near surface initiated fatigue failure. Fatigue tests in conjunction with the stress model are badly needed to further extend our knowledge of the role of low levels of friction on fatigue.

Figure 16 shows a shear stress plot of τ_{xy} versus τ_{zx} for the plane of maximum shear stress at the center of contact very near the surface. The magnitude of the stress reversals envelope ($\approx$ .6) is very consistent with the Smith-Liu[5] computations and further illustrates the effect of severe friction (f = .33) on fatigue inducing stresses. However, the effect of friction on these stresses is not a factor at lower friction.

In conclusion, it can be said that based on the computer models discussed herein, low friction coefficient (f < .1) do not alter the fatigue stresses. At higher friction levels, changes will occur, but these cannot explain the observed effect of friction on fatigue. Other factors such as non-Hertzian pressures, thermal stress, and nonsymmetric tractions should then be included to understand the roll of friction on fatigue stress.

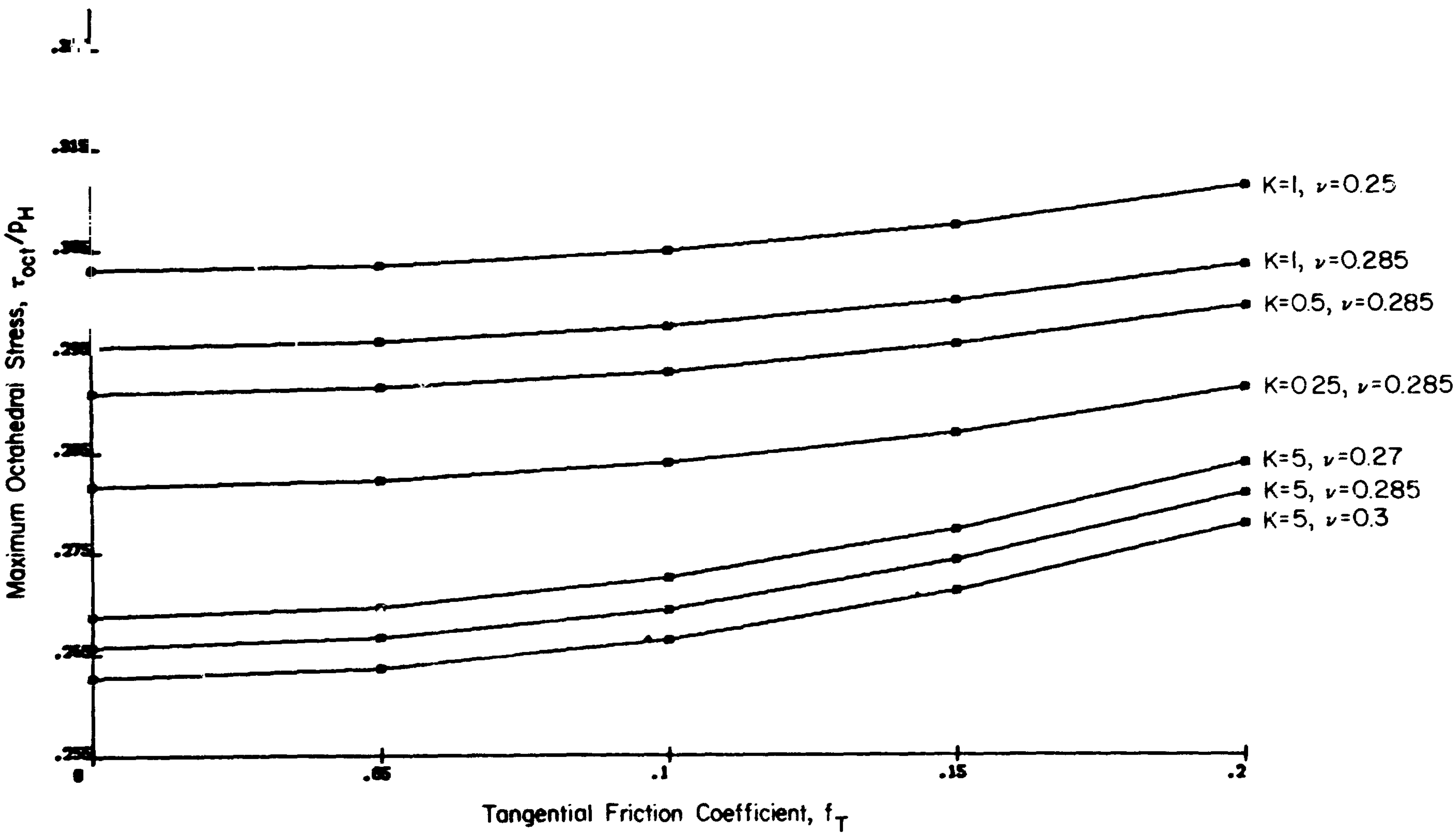

FIGURE 13. EFFECT OF FRICTION ON MAXIMUM OCTAHEDRAL SHEAR STRESS (T-Model)

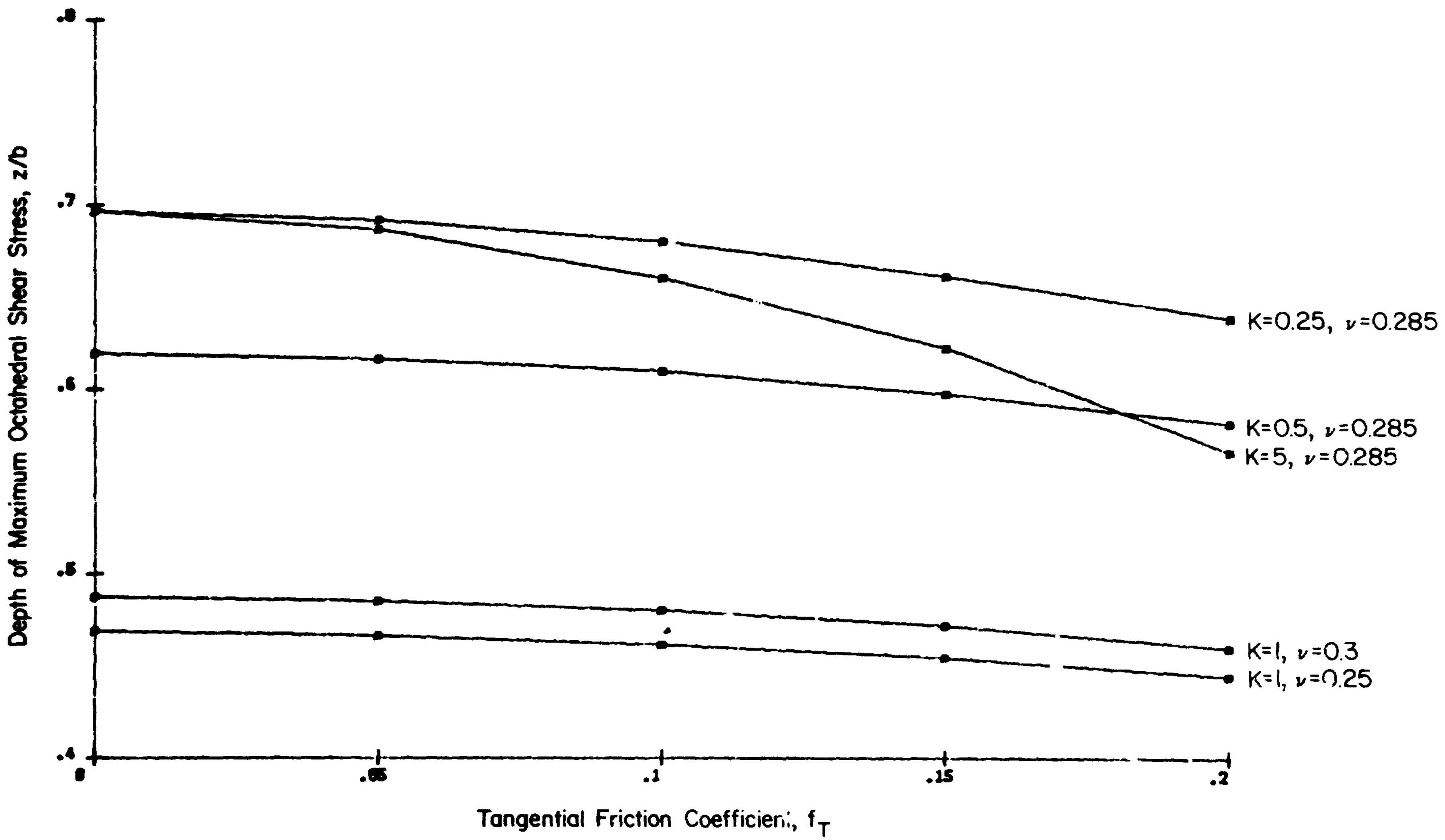

FIGURE 14. EFFECT OF FRICTION ON DEPTH OF MAXIMUM OCTAHEDRAL STRESS

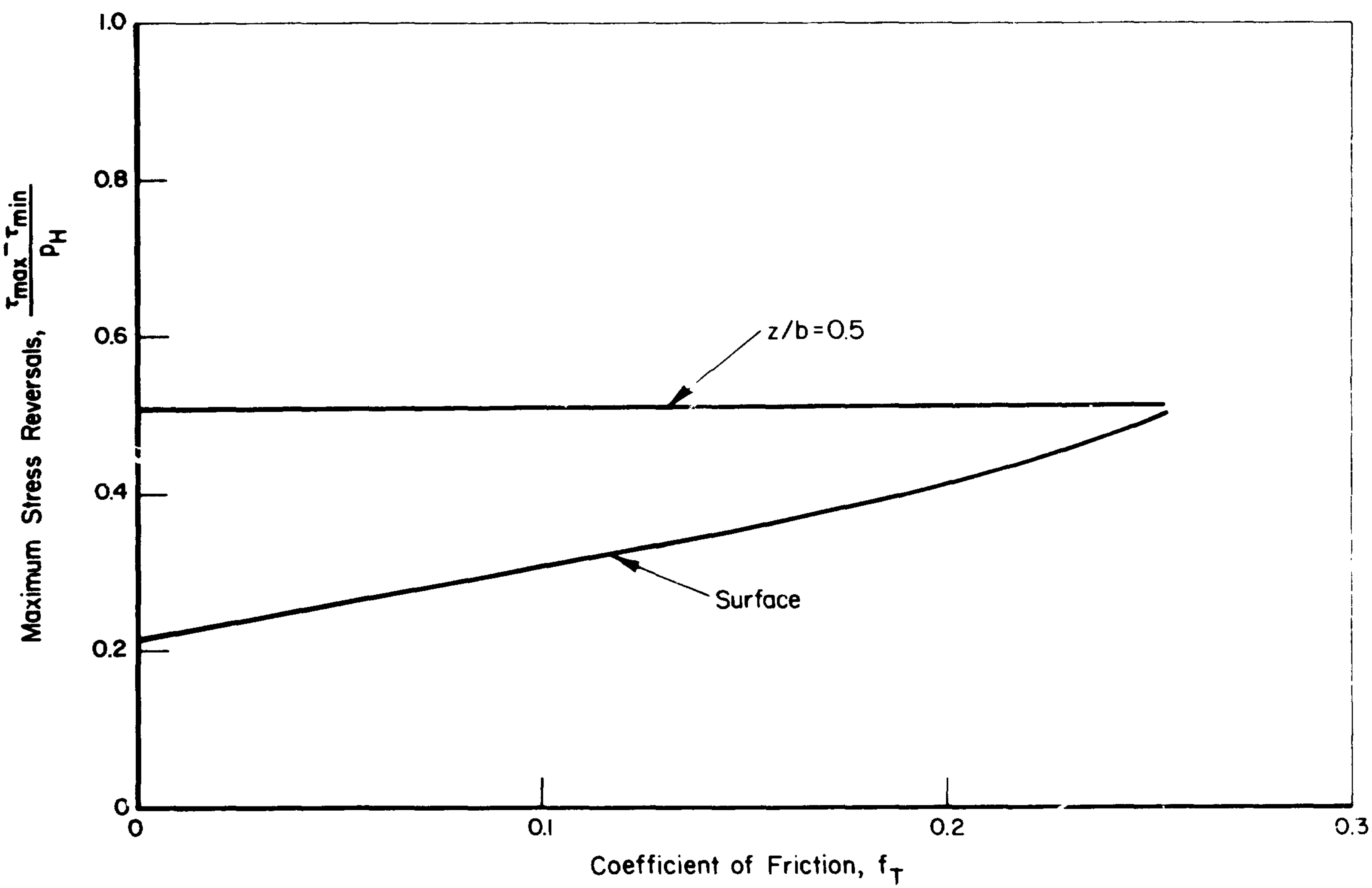

FIGURE 15. EFFECT OF FRICTION ON MAXIMUM STRESS REVERSALS
($K = 0$, $f_A = 0$, $\nu = .285$, B-Model)

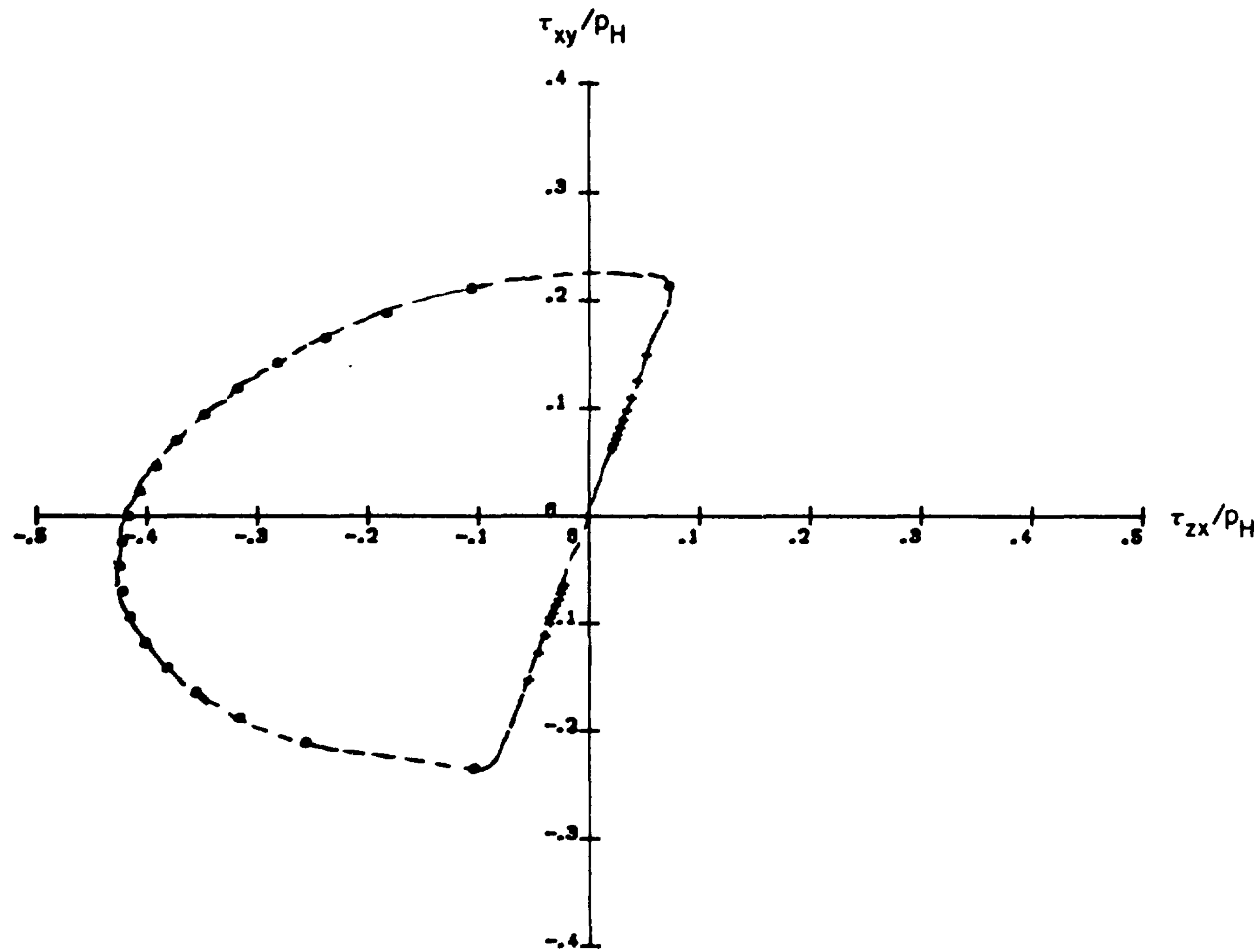

FIGURE 16. ILLUSTRATION OF VARIATION OF SHEAR STRESS ON PLANE OF MAXIMUM SHEARING STRESS
($z/b = 0$, $K = 0$, $\nu = .25$, $f_T = .333$ T-Model)

SUMMARY

The performance life of traction drives can be a very important factor in evaluating the overall effectiveness of the drive concept. Intuitively, this life should be heavily related to the state-of-stress in the elements as a result of high loads and tractions. The purpose of the project has been to develop a mathematical tool for evaluating this stress-state. Two independent, but similar, approaches (one at Battelle and one by Tevaarwerk) to developing the stress model have been pursued. Essentially, the models involve the computations of subsurface shear stresses (and stress reversals) as a result of normal and frictional loadings. Where possible the models have been checked against existing theory and against each other.

One use of the stress models has been to evaluate fatigue test methodology for a rolling contact (RC) fatigue tester. The standard RC tester consists of a small driven cylinder loaded between two larger crowned cylinders. The RC tester is a candidate device to evaluate the effect of traction on fatigue, either by driving the crowned rollers (tangential slip) or by simply skewing the rollers (axial slip); the skewing technique would be easier. The stress model was used to evalute the effect of lubricated type tractions on stresses for a typical RC configuration.

The general conclusion from the RC evaluations was that the fatigue inducing stresses (shear stress) reversals and depth of shear stress are not seriously altered by tractions (axial or tangential) which are typical of lubricated contacts. There are some changes in the stress field, but these are difficult to relate to fatigue. To further explore the effect of friction on stress, additional computer cases have been evaluated.

The general conclusions from additional computer analyses is that friction coefficients of the order of 0.25 are required to materially alter the state of fatigue inducing stresses; this is much larger than would occur in lubricated contact. This implies then, that other effects not incorporated in the current stress-models should be included. These effects include non-Hertzian stresses distributions and thermal stresses. Both of these effects can impose nonsymmetrical (about the center of contact) shear stresses and thus will produce shear stress reversals which will superimpose on the normal and friction stresses.

REFERENCES

(1) Lundberg, G. and Palmgren, A., "Dynamic Capacity of Rolling Bearings", Ing. Vetanskap, Akad.-Handl., No. 196, 1947.

(2) Coy, J. J., Loewenthal, S.H., and Zaretsky, E.V., "Fatigue Life Analysis for Traction Drives with Applications to a Torodial-Type Geometry", NASA TND-8362.

(3) Hertz, Heinrich, Miscellaneous Papers. Part V - The Contact of Elastic Solids, the MacMillan Company (London), pp 146-162, 1896.

(4) Harris, Tedric A., Rolling Bearing Analysis, John Wiley & Sons, Inc., 1966.

(5) Smith, T. O. and Liu, C. K., "Stresses Due to Tangential and Normal Loads on an Elastic Solid with Application to Some Contact Stress Problems", Trans. ASME, J.O.A.M., pp 157-166, June 1953.

(6) Hamilton, G. M. and Goodman, L. E., "The Stress Field Created by a Circular Sliding Contact", Trans. ASME, J.O.A.M., 33, E, pp 371-376, 1966.

(7) Kuznetsov, Ye. A., "The Superposition Principle in the Solution of Contact Friction Stress Problems", Wear, 50, pp 183-189, 1978.

(8) Shames, I. H., Mechanics of Deformable Solids, Prentice Hall, Englewood Cliffs, N.J., pp 15-29, 1964.

(9) Mindlin, R. D., "Force at a Point in the Interior of a Semi-Infinite Solid", Physics, Vol. 7, pp 195-202, May 1936.

APPENDIX A

COMPUTATIONS OF THE STRESS TENSOR

APPENDIX A

COMPUTATIONS OF THE STRESS TENSOR

Stress Due to Point Loads

The state of stress at any point on or beneath the surface of a system under concentrated contact is quite complex. To define this stress state at each point requires the computations of nine components of the stress tensor as related to contact pressures and tractions. The effect of pressures and tractions on stress were developed by Mindlin[9] for point loadings on the surface of a semiinfinite body using the coordinate system of Figure A-1, and letting $R^2 = x^2 + y^2 + z^2$. These equations appear as follows.

Normal Load.

$$\sigma'_{xN} = \frac{P_N}{2\pi}\left\{\frac{(1-2\nu)z}{R^3} - \frac{3x^2 z}{R^5} - \frac{(1-2\nu)}{R(R+z)}\left[1 - \frac{x^2}{R(R+z)} - \frac{x^2}{R^2}\right]\right\} \quad ,\text{(A-1)}$$

$$\sigma'_{yN} = \frac{P_N}{2\pi}\left\{\frac{(1-2\nu)z}{R^3} - \frac{3y^2 z}{R^5} - \frac{(1-2\nu)}{R(R+z)}\left[1 - \frac{y^2}{R(R+z)} - \frac{y^2}{R^2}\right]\right\} \quad ,\text{(A-2)}$$

$$\sigma'_{z_N} = -\frac{3 P_N z^3}{2\pi R^5} \quad , \qquad \text{(A-3)}$$

$$\tau'_{zy_N} = \tau'_{yz_N} = -\frac{3 P_N y z^3}{2\pi R^5} \quad , \qquad \text{(A-4)}$$

$$\tau'_{xz_N} = \tau'_{zx_N} = -\frac{3}{2\pi}\frac{P_N\, x\, z^2}{R^5} , \qquad \text{(A-5)}$$

$$\tau'_{yx_N} = \tau'_{xy_N} = \frac{P_N\, xy}{2\pi} \quad -\frac{3z}{R^5} + \frac{(1 - 2\nu)(2R + z)}{R^3(R + z)^2} . \qquad \text{(A-6)}$$

Tangential Load.

$$\sigma'_{x_T} = \frac{P_T\, x}{2\pi} \quad \frac{1 - 2\nu}{R^3} - \frac{3x^2}{R^5} - \frac{(1 - 2\nu)}{R(R + z)^2} \quad 3 - \frac{x^2(3R + z)}{R^2(R + z)} , \qquad \text{(A-7)}$$

$$\sigma'_{y_T} = \frac{P_T\, x}{2\pi} \quad \frac{1 - 2\nu}{R^3} - \frac{3y^2}{R^5} - \frac{(1 - 2\nu)}{R(R + z)^2} \quad 1 - \frac{y^2(3R + z)}{R^2(R + z)} , \qquad \text{(A-8)}$$

$$\sigma'_{z_T} = -\frac{3P_T}{2\pi}\frac{x\, z^2}{R^5} , \qquad \text{(A-9)}$$

$$\tau'_{zy_T} = \tau'_{yz_T} = -\frac{3P_T\, xyz}{2\pi\, R^5} , \qquad \text{(A-10)}$$

$$\tau'_{xz_T} = \tau'_{zx_T} = -\frac{3P_T\, x^2 z}{2\pi\, R^5} , \qquad \text{(A-11)}$$

$$\tau'_{yx_T} = \tau'_{xy_T} = \frac{P_T\, y}{2\pi} \quad -\frac{3x^2}{R^5} - \frac{(1 - 2\nu)}{R(R + z)^2} \quad 1 - \frac{x^2(3R + z)}{R^2(R + z)} . \qquad \text{(A-12)}$$

Axial Load.

$$\sigma'_{x_A} = \frac{P_A\, y}{2\pi} \quad \frac{1 - 2\nu}{R^3} - \frac{3x^2}{R^5} - \frac{(1 - 2\nu)}{R(R + z)^2} \quad 1 - \frac{x^2(3R + z)}{R^2(R + z)} , \qquad \text{(A-13)}$$

$$\sigma'_{y_A} = \frac{P_A\, y}{2\pi}\left\{\frac{1-2\nu}{R^3} - \frac{3y^2}{R^5} - \frac{(1-2\nu)}{R(R+z)^2}\left[3 - \frac{y^2(3R+z)}{R^2(R+z)}\right]\right\} , \qquad (A-14)$$

$$\sigma'_{z_A} = -\frac{3\,P_A\, y\, z^2}{2\pi\, R^5} , \qquad (A-15)$$

$$\tau'_{zx_A} = \tau'_{xz_A} = -\frac{3P_A\, xyz}{2\pi\, R^5} , \qquad (A-16)$$

$$\tau'_{zy_A} = \tau'_{yz_A} = -\frac{3P_A\, y^2 z}{2\pi\, R^5} , \qquad (A-17)$$

$$\tau'_{xy_A} = \tau'_{yx_A} = \frac{P_A\, x}{2\pi}\left\{-\frac{3y^2}{R^5} - \frac{(1-2\nu)}{R(R+z)^2}\left[1 - \frac{y^2(3R+z)}{R^2(R+z)}\right]\right\} . \qquad (A-18)$$

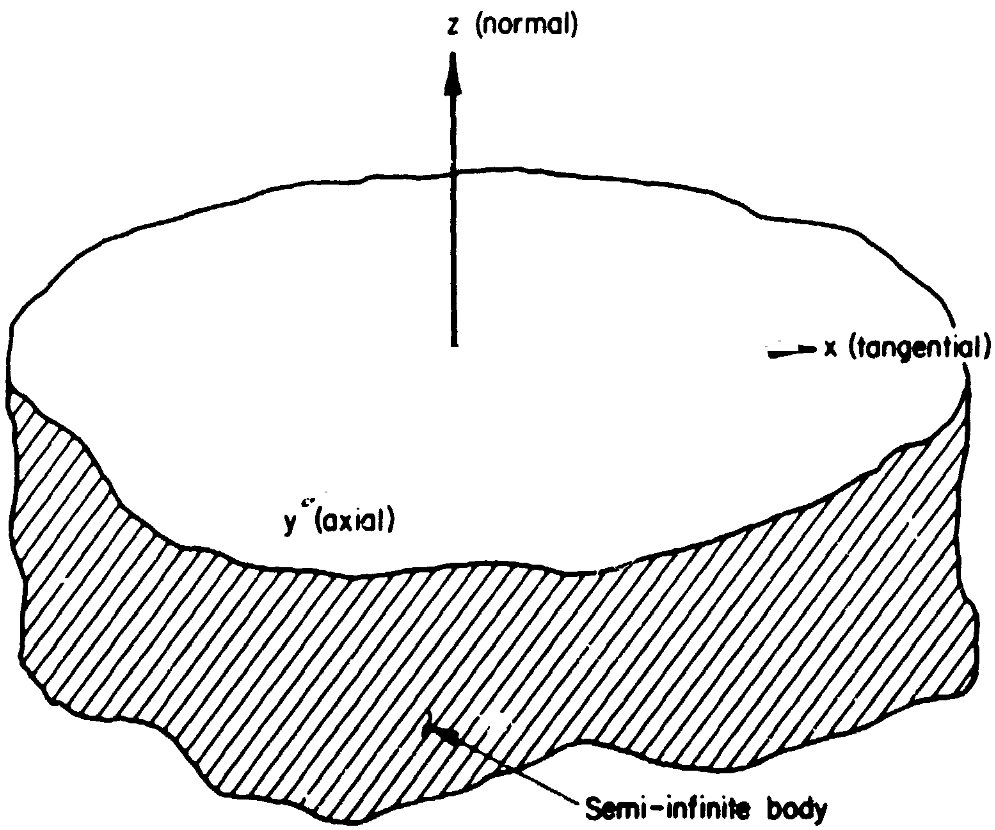

FIGURE A-1. COORDINATE SYSTEM FOR STRESS COMPUTATIONS

Hertzian Pressures and Surface Tractions

For a point on the surface, the normal load could be written

$P_N = p\,dxdy$ where p is the local pressure (A-19)

Also, $P_T = pf_T\,dxdy$ and (A-20)

$P_A = pf_A\,dxdy$ (A-21)

where f_T and f_A are the effective coefficients of friction acting tangential or axially to the surface.

If the surface were subjected to a Hertzian pressure distribution, the pressure could be expressed (see Figure A-2):

$$p = p_H \sqrt{1 - \frac{(x - x_1)^2}{b^2} - \frac{(y - y_1)^2}{a^2}} \; , \tag{A-22}$$

where p_H is the maximum Hertz pressure, a and b are the major and minor axes of the contact ellipse, x and y are the coordinates with origins at the center of the ellipse and x_1 and y_1 are locations of the point load relative to the center of the Hertz ellipse. The Battelle analyses were restricted to the case where $y_1 = 0$. Tevaarwerk allowed y_1 to be a variable and found $y_1 = 0$ to be the interesting region.

The general approach for determining the nine components of the stress tensor at any point can be written

$$\sigma_{ij} = p_H \iint_A \left[\frac{\sigma'_{ij_N}}{P_N} + \frac{f_T\sigma'_{ij_T}}{P_T} + \frac{f_A\sigma'_{ij_A}}{P_A}\right] \sqrt{1 - \frac{(x - x_1)^2}{b^2} - \frac{y^2}{a^2}} \; dxdy \; , \tag{A-23}$$

where σ_{ij} represents nine components of the stress tensor* for Hertzian pressures and various frictional forces and σ'_{ij} are the results of Mindlin's analyses (discussed in the previous section). In further computations, we

---

* In tensor notation σ_{ij} implies σ_{11}, σ_{12}, σ_{13}, σ_{21} . . .σ_{33}, where σ_{11} is σ_x, σ_{12} is τ_{xy}, σ_{22} is σ_y, σ_{23} is τ_{yz}, etc.

shall use $\overline{\sigma}_{ij} = \sigma_{ij}/p_H$ such that all computations will be normalized on the Hertz maximum pressures.

It would serve no purpose to show all substitutions of Mindlin's equations into the general stress tensor equation. It can be noted that any of Mindlin's equations containing the term y^n (n odd) will produce a zero integral since the integration involves that function times the even Hertz pressure over the whole pressure region for $y_1 = 0$. As an example of how the substitution occurs, consider the normal stress $\overline{\sigma}_z$ for f_T and $f_A = 0$.

$$\overline{\sigma}_z \equiv \overline{\sigma}_{33} = \int_{-a}^{a} \int_{L}^{U} \frac{3}{2\pi} \frac{z^3}{R^5} \sqrt{1 - \left(\frac{x - x_1}{b}\right)^2 - \frac{y^2}{a^2}} \, dxdy \quad , \qquad \text{(A-24)}$$

where the lower limit $L = x_1 - b\sqrt{1 - \frac{y^2}{a^2}}$, and

the upper limit $U = x_1 + b\sqrt{1 - \frac{y^2}{a^2}}$.

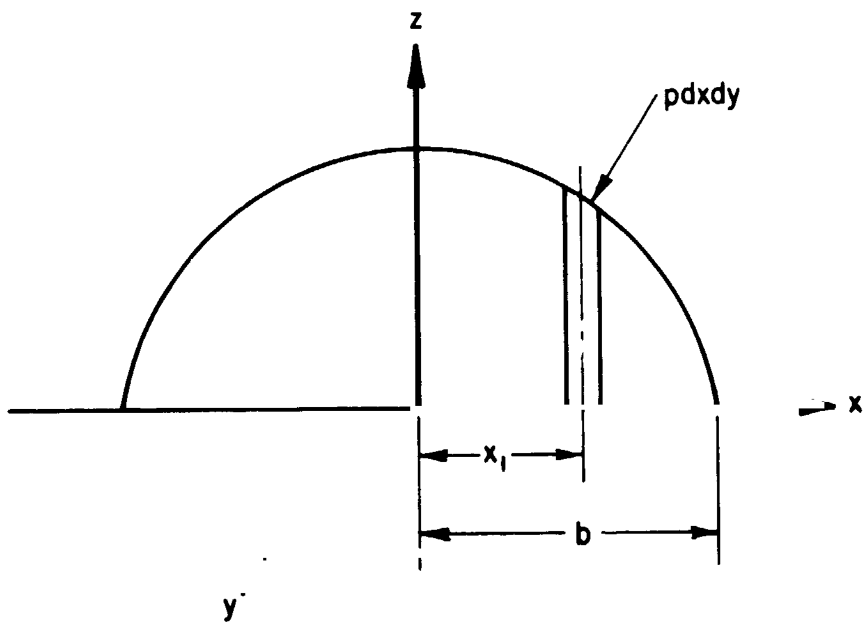

FIGURE A-2. LOADING CHARACTERIZED BY HERTZIAN ELLIPSE

Scaling the Stress Tensor Equations

The following substitutions were used to facilitate computations:

$$\bar{z} = z/b \quad \xi = x/z \quad \eta = y/z \quad K = b/a \quad \text{and} \quad \bar{x}_1 = x_1/b \quad .$$

With these substitutions Equation A-24 appears

$$\bar{\sigma}_z = \frac{3}{2\pi} \int_{-1/K\bar{z}}^{1/K\bar{z}} \int_{\bar{L}}^{\bar{U}} \frac{1}{\bar{R}^5} \sqrt{1 - (\bar{z}\xi - \bar{x}_1)^2 - (K\bar{z}\xi)^2} \; d\xi d\eta \quad , \qquad \text{(A-25)}$$

where

$$\bar{L} = \bar{x}_1/\bar{z} - 1/\bar{z}\sqrt{1 - (\bar{z}K\eta)^2} \quad ,$$

$$\bar{U} = \bar{x}_1/\bar{z} + 1/\bar{z}\sqrt{1 - (\bar{z}K\eta)^2} \quad , \text{ and}$$

$$\bar{R} = \sqrt{\xi^2 + \eta^2 + 1} \quad .$$

This type of substitution permitted reasonable computations near $\bar{z} = 0$.

In the computer solution

$$\bar{\sigma}_z = \frac{3}{2\pi} (2) \int_0^{\infty} \int_{-\infty}^{\infty} \frac{\sqrt{A}}{R^5} \; d\xi d\eta \quad , \qquad \text{(A-26)}$$

where

$$A = \begin{cases} 1 - (\bar{z}\xi - \bar{x}_1)^2 - (K\bar{z}\eta)^2 & \text{(A positive)} \\ 0 & \text{(otherwise)} \quad . \end{cases}$$

All other stress components were treated in the same manner using the general expression

$$\bar{\sigma}_{ij} = 2 \int_{0}^{\infty} \int_{-\infty}^{\infty} \left[\frac{\bar{\sigma}'_{ijN}}{P_N} + \frac{f_T \bar{\sigma}'_{ijT}}{P_T} + \frac{f_A \bar{\sigma}'_{ijA}}{P_A} \right] \sqrt{A} \; d\xi \; d\eta \quad , \qquad \text{(A-27)}$$

where by substituting $\xi = x$, $\eta = y$ and $z = 1$, all equations for σ'_{ij} become the equations for $\bar{\sigma}'_{ij}$.

Review

This is the most involved section in the report and may be difficult for the reader to readily grasp. Basically, all it involves is to take Mindlin's equations (A-1 - A-18), replace x with ξ, y with η, and z with 1 and integrate equation A-27. For example, suppose we want to calculate $\bar{\sigma}_{13} = \tau_{xz}$ from the normal load equation

$$\frac{\bar{\sigma}'_{13\ N}}{P_N} = - \frac{3}{2\pi} \frac{\xi}{R^5} \quad \text{(Equation A-5)} \quad . \qquad \text{(A-28)}$$

From the tangential load equation

$$\frac{\bar{\sigma}'_{13\ T}}{P_T} = - \frac{3}{2\pi} \frac{\xi^2}{R^5} \quad \text{(Equation A-11)} \quad . \qquad \text{(A-29)}$$

From the axial load equation

$$\frac{\bar{\sigma}'_{13\ A}}{P_A} = - \frac{3}{2\pi} \frac{\xi\eta}{R^5} \quad \text{(Equation A-16)} \quad , \qquad \text{(A-30)}$$

where $\bar{R} = \sqrt{1 + \xi^2 + \eta^2}$.

Equation A-27 then becomes

$$\bar{\sigma}_{13} = -2 \int_{0}^{\infty} \int_{-\infty}^{\infty} \frac{3\ \bar{R}^{5}}{2\pi} \left[\xi + \xi^{2} + \xi\eta\right] \sqrt{A}\ d\xi\ d\eta \quad . \qquad \text{(A-31)}$$

This equation can be solved by numerical computation. In the Battelle computations, the integral on ξ was performed by a Gaussian quadrature approach and the y integration was performed by a Trapezoidal rule.

Check of Numerical Solution

Hamilton and Goodman[6] developed an exact solution for circular contacts (K = 1). The numerical solution is compared with the exact solution in Table A-1; the exact solution was generated as a part of the work of Tevaarwerk. The agreement tends to verify the numerical accuracy.

Smith & Liu[5] developed an exact solution for line contact (K = 0). The numerical solution is compared with the exact solution in Table A-2.

TABLE A-1. COMPARISON OF NUMERICAL SOLUTION WITH EXACT SOLUTION FOR K = 1[6]
($\nu = 0.3$, $f_T = f_A = 0$)

		σ_x		σ_y		σ_z		τ_{xy}		τ_{yz}		τ_{xz}	
x/b	z/b	Num	Exact	Num	Exact	Num	Exact	Num	Exact	Num	Exact	Num	Exact
.1	-.8	-.305	-.300	-.361	-.356	-.579	-.573	0	0	0	0	.121	.119
	-.5	-.507	-.501	-.532	-.524	-.862	-.853	0	0	0	0	.057	.056
	-.3	-.581	-.575	-.591	-.583	-.953	-.943	0	0	0	0	.031	.031
	0	-.620	-.614	-.623	-.614	-1.00	-.99	0	0	0	0	0	0
	.3	-.581	-.575	-.591	-.583	-.953	-.943	0	0	0	0	-.031	-.031
	.5	-.507	-.501	-.532	-.524	-.861	-.853	0	0	0	0	-.057	-.056
	.8	-.305	-.300	-.360	-.356	-.579	-.573	0	0	0	0	-.121	-.119
.4	-.8	-.184	-.184	-.128	-.129	-.450	-.445	0	0	0	0	.213	.212
	-.5	-.212	-.212	-.198	-.199	-.717	-.709	0	0	0	0	.150	.149
	-.3	-.235	-.235	-.230	-.231	-.818	-.809	0	0	0	0	.090	.090
	0	-.252	-.250	-.249	-.250	-.871	-.862	0	0	0	0	0	0
	.3	-.235	-.235	-.230	-.231	-.817	-.809	0	0	0	0	-.090	-.090
	.5	-.212	-.212	-.198	-.199	-.717	-.709	0	0	0	0	-.150	-.149
	.8	-.185	-.184	-.128	-.129	-.450	-.445	0	0	0	0	-.213	-.212

TABLE A-2. COMPARISON OF NUMERICAL SOLUTION WITH EXACT SOLUTION FOR K = 0[5]
(ν = .285, f_A = 0)

			σ_x		σ_y		σ_z		τ_{xy}		τ_{yz}		τ_{yz}	
f_T	z/b	x/b	Num	Exact	Num	Exact	Num	Exact	Num	Exact	Num	Exact	Num	Exact
0	.5	-.8	-.298	-.299	-.240	-.227	-.506	-.500	0	0	0	0	.249	.247
		-.5	-.311	-.313	-.314	-.301	-.751	-.745	0	0	0	0	.180	.176
		-.3	-.328	-.329	-.346	-.334	-.850	-.842	0	0	0	0	.109	.107
		0	-.342	-.342	-.367	-.352	-.905	-.894	0	0	0	0	0	0
		.3	-.328	-.329	-.346	-.334	-.850	-.842	0	0	0	0	-.109	-.107
		.5	-.311	-.313	-.314	-.301	-.751	-.745	0	0	0	0	-.180	-.176
		.8	-.298	-.299	-.240	-.227	-.506	-.500	0	0	0	0	-.249	-.247
.15	.5	-.8	-.228	-.229	-.209	-.200	-.468	-.462	0	0	0	0	.203	.202
		-.5	-.259	-.263	-.290	-.280	-.724	-.718	0	0	0	0	.133	.129
		-.3	-.295	-.297	-.331	-.320	-.834	-.826	0	0	0	0	.059	.057
		0	-.342	-.342	-.367	-.353	-.905	-.894	0	0	0	0	-.052	-.051
		.3	-.361	-.362	-.360	-.348	-.867	-.858	0	0	0	0	-.159	-.157
		.5	-.363	-.364	-.337	-.324	-.779	-.771	0	0	0	0	-.227	-.222
		.8	-.369	-.369	-.272	-.260	-.543	-.536	0	0	0	0	-.295	-.292

APPENDIX B

SOURCE LISTING FOR BATTELLE STRESS MODEL

```
      PROGRAM SUBSTS(INPUT,OUTPUT,TAPE 1)
      COMMON/F/ ISTRSS,X1(22,1),GNU,Z,Y,XK,FT,FA,MX
      COMMON/C/ STRSS(3,3,22)
      DIMENSION AN(3,3),ASM(3,22),AS(3,22),BN1(3),BN2(3)
     1,CN1(3,22),CN2(3,22),CN3(3,22)
      REWIND 1
      BN1(1)=.70711
      BN1(2)=0.
      BN1(3)=-.70711
      BN2(1)=.57735
      BN2(2)=.57735
      BN2(3)=.57735
      CN3(1,1)=0.
      CN3(2,1)=0.
      CN3(3,1)=1.
      SIGN=+1.
      SIGNA=+1.
8     PRINT 6
6     FORMAT( * INPUT,ASPECT RATIO,NU,Z,FT,FA,X-POSS,CASE-NO*)
      READ*,XK,GNU,Z,FT,FA,MX,NCASE
      IF(XK.LT.0.) GO TO 7
      WRITE(1,13) NCASE
13    FORMAT(///,50X,* CASE NUMBER=*,I8,///)
      WRITE(1,9) XK,GNU,Z,FT,FA
      PRINT 9,XK,GNU,Z,FT,FA
9     FORMAT( * K=*,E12.5, * NU=*,E12.5,* Z=*,E12.5,* FT=*,E12.5,* FA=*,
     1E12.5,//)
      TMXXM=TMXXO=TAURVM=TAURVO=0.
      IF(XK.LT.1.E-6) CALL STRSSC(1)
      IF(XK.GT.1.E-6) CALL STRSSC(6)
      WRITE(1,12)
12    FORMAT(*  IX        SXX           SYY           SZZ          SXY
     1SYZ          SXZ           S1           S2           S3      X-POS
     1*//)
      DO 1 IX=1,MX
      CALL PRINC(STRSS,IX,S1,S2,S3)
      CALL ANGLP(STRSS,S1,S2,S3,AN,IX,SIGNA)
      CALL ANGTRAN(AN,BN1,CN1,IX)
      CALL ANGTRAN(AN,BN2,CN2,IX)
      WRITE(1,11) IX,STRSS(1,1,IX),STRSS(2,2,IX),STRSS(3,3,IX),
     1STRSS(1,2,IX),STRSS(2,3,IX),STRSS(1,3,IX),S1,S2,S3,X1(IX,1)
11    FORMAT(I5,10E12.5)
1     CONTINUE
      WRITE(1,28)
28    FORMAT(//,45X,* FATIGUE SHEAR STRESS SUMMARY * //)
      DO 21 IXRF=1,MX
      XRF=X1(IXRF,1)
      CALL RVSTRS(STRSS,CN1,ASM,TRVM,TMAX,IXRF,SIGN)
      PRINT 99,TMAX
99    FORMAT( * TMAX=*,E12.5)
      IF(ABS(TRVM).GT.ABS(TAURVM)) TAURVM=TRVM
      IF(ABS(TMAX).GT.ABS(TMXXM)) 22,23
22    TMXXM=TMAX
      IXRFM=IXRF
      SIGN=-1.
23    CALL RVSTRS(STRSS,CN2,AS,TRVMO,TMAXO,IXRF,SIGN)
      IF(ABS(TRVMO).GT.ABS(TAURVO)) TAURVO=TRVMO
      IF(ABS(TMAXO).GT.ABS(TMXXO))24,25
24    TMXXO=TMAXO
      IXRFO=IXRF
25    CONTINUE
      PRINT 29,IXRF,TRVM,TMAX,TRVMO,TMXXO
29    FORMAT(I5,4E14.5)
```

```
21    CONTINUE
      WRITE(1,15)
15    FORMAT(//,20X,* PLANE OF MAX SHEAR STRESS*//)
      WRITE(1,18) TMXXM,CN1(1,IXRFM),CN1(2,IXRFM),CN1(3,IXRFM),X1(IXRFM,
     1,E13.5,* X-REF=*,E13.5)
      WRITE(1,19) TAURVM,ASM(1,IXRFM),ASM(2,IXRFM),ASM(3,IXRFM)
19    FORMAT( * TAU REVERSING=*,E13.5,* AS(1)=*,E13.5,* AS(2)=*,E13.5,
     1*AS(3)=*,E13.5)
      WRITE(1,16)
16    FORMAT(//,20X,* PLANE OF MAX OCT SHEAR STRESS *//)
      WRITE(1,18) TMXXO,CN2(1,IXRFO),CN2(2,IXRFO),CN2(3,IXRFO),X1(IXRFO,
     11)
      WRITE(1,19) TAURVO,AS(1,IXRFO),AS(2,IXRFO),AS(3,IXRFO)
      CALL RVSTRS(STRSS,CN3,AS,TRVM,TMAX,1,SIGN)
      WRITE(1,17)
17    FORMAT(//,20X,* PLANE OF REVERSING SHEAR STRESS *//)
      WRITE(1,18) TMAX,CN3(1,1),CN3(2,1),CN3(3,1)
      WRITE(1,19) TRVM,AS(1,1),AS(2,1),AS(3,1)
      WRITE(1,20)
20    FORMAT(1H1)
      GO TO 8
7     CONTINUE
      END
        SUBROUTINE STRSSC(IFLAG)
      COMMON/F/ IS,X1(22,1),GNU,Z,Y,XK,FT,FA,MX1
      COMMON/C/ STRSS(3,3,22)
      DIMENSION FI(22,17),GINT(22),ICALC(22),TEMP1(22),FX(22),FIY(17)
     1,Y1(17)
      PI=3.14159
      MY=17
      MX=MX1
      CALL XPOS
      IF(IFLAG.EQ.1) GO TO 10
      DO 9 ISTRSS=1,6
      IS=ISTRSS
      DO 4 JY=1,MY
      IF(JY.EQ.1) Y=0.
      IF(JY.EQ.2) Y=.2
      IF(JY.EQ.3) Y=.4
      IF(JY.EQ.4) Y=.6
      IF(JY.EQ.5) Y=.8
      IF(JY.EQ.6) Y=1.2
      IF(JY.EQ.7) Y=1.6
      IF(JY.EQ.8) Y=2.
      IF(JY.EQ.9) Y=2.5
      IF(JY.EQ.10) Y=3.
      IF(JY.EQ.11) Y=4.
      IF(JY.EQ.12) Y=6.
      IF(JY.EQ.13) Y=8.
      IF(JY.EQ.14) Y=10.
      IF(JY.EQ.15) Y=20.
      IF(JY.EQ.16) Y=30.
      IF(JY.EQ.17) Y=50.
      Y1(JY)=Y
      BL=-2./Z
      IF(BL.LT.-20.) BL=-20.
      BU=-BL
      IELE=1
      CALL GAUSS(MX,1,20,1,1.E-3,1.E-3,BL,BU,GINT,ICALC,TEMP1,FX)
      DO 5 IX=1,MX
      FI(IX,JY)=GINT(IX)
5     CONTINUE
4     CONTINUE
```

```
      DO 6 IX=1,MX
      DO 8 IY=1,MY
 8    FIY(IY)=FI(IX,IY)
      CALL YINT(FIY,Y1,SIG1,MY)
      IF(IS.EQ.1) STRSS(1,1,IX)=SIG1
      IF(IS.EQ.2) STRSS(2,2,IX)=SIG1
      IF(IS.EQ.3) STRSS(3,3,IX)=SIG1
      IF(IS.EQ.4) STRSS(1,2,IX)=STRSS(2,1,IX)=SIG1
      IF(IS.EQ.5) STRSS(2,3,IX)=STRSS(3,2,IX)=SIG1
      IF(IS.EQ.6) STRSS(1,3,IX)=STRSS(3,1,IX)=SIG1
 6    CONTINUE
 9    CONTINUE
      RETURN
 10   CONTINUE
      DO 12 ISTRSS=1,5
      IS=ISTRSS
      DO 11 IX=1,MX
      X=X1(IX,1)
      XK1=(1.+X)**2+Z**2
      XK2=(1.-X)**2+Z**2
      C1=SQRT(XK2/XK1)
      C2=SQRT(2.*C1+(XK1+XK2-4.)/XK1)
      SI=PI/XK1*(1.-C1)/C1/C2
      SIB=PI/XK1*(1.+C1)/C1/C2
      SXN=-1./PI*Z*((1.+2.*X**2+2.*Z**2)*SIB-2.*PI-3.*X*SI)
      SZN=-Z/PI*(SIB-X*SI)
      TXZN=-1./PI*Z**2*SI
      CTZ=-1./PI*((1.+2.*X**2+2.*Z**2)*Z*SIB-2.*PI*Z-3.*X*Z*SI)
      TXZT=FT*CTZ
      TYZT=FA*CTZ
      CXT=-1./PI*((2.*X**2-2.-3.*Z**2)*SI+2.*PI*X+2.*(1.-X**2-Z**2)*X
     1*SIB)
      SXT=FT*CXT
      SYT=FA*CXT
      SZT=-(FT+FA)/PI*Z**2*SI
      IF(IS.EQ.1) STRSS(1,1,IX)=SXN+SXT
      IF(IS.EQ.2) STRSS(2,2,IX)=GNU*(SXN+SXT+SZN+SZT)+SYT
      IF(IS.EQ.3) STRSS(3,3,IX)=SZN+SZT
      IF(IS.EQ.4) STRSS(1,2,IX)=STRSS(2,1,IX)=0.
      IF(IS.EQ.5) STRSS(2,3,IX)=STRSS(3,2,IX)=TYZT
      IF(IS.EQ.6) STRSS(1,3,IX)=STRSS(3,1,IX)=TXZN+TXZT
 11   CONTINUE
 12   CONTINUE
      RETURN
      END
        SUBROUTINE YINT(FI,Y1,SIG1,MY)
      DIMENSION FI(17),Y1(17)
      C1=FI(1)*(Y1(2)-Y1(1))
      C2=FI(MY)*(Y1(MY)-Y1(MY-1))
      SUM=0.
      MY1=MY-1
      DO 1 I=2,MY1
 1    SUM=SUM+FI(I)*(Y1(I+1)-Y1(I-1))
      SIG1=C1+C2+SUM
      RETURN
      END
        SUBROUTINE FEVAL(X,FX,JF,ICALC)
      COMMON/F/ ISTRSS, X1(22,1),GNU,ZB,Y,XK,FT,FA,MX
      DIMENSION FX(22),ICALC(22)
      PI=3.14159
      X2=X**2
      Y2=Y**2
      GNU1=1.-2.*GNU
```

```
      R=SQRT(X**2+Y**2+1.)
      R2=R**2
      R3=R**3
      R5=R**5
      RZ=R+1.
      IF(ISTRSS.EQ.1) 1,2
 1    C1=(GNU1/R3-3.*X2/R5-GNU1/R/RZ*(1.-X2/R/RZ-X2/R2))/2./PI
      C2=(GNU1/R3-3.*X2/R5-GNU1/R/RZ**2*(3.-X2*(3.*R+1.)/R2/RZ))/2./PI*X
      C3=0.
      GO TO 10
 2    IF(ISTRSS.EQ.2) 3,4
 3    C1=(GNU1/R3-3.*Y2/R5-GNU1/R/RZ*(1.-Y2/R/RZ-Y2/R2))/2./PI
      C2=(GNU1/R3-3.*Y2/R5-GNU1/R/RZ**2*(1.-Y2*(3.*R+1.)/R2/RZ))*X/2./PI
      C3=0.
      GO TO 10
 4    IF(ISTRSS.EQ.3) 5,6
 5    C1=-3./R5/2./PI
      C2=-3./2./PI*X/R5
      C3=0.
      GO TO 10
 6    IF(ISTRSS.EQ.4) 7,8
 7    C1=0.
      C2=0.
      C3=(-3.*X2/R5-GNU1/R/RZ**2*(1.-X2*(3.*R+1.)/R2/RZ))/2./PI*X
      GO TO 10
 8    IF(ISTRSS.EQ.5) 9,11
 9    C1=0.
      C2=0.
      C3=-3./2./PI*Y2/R5
      GO TO 10
 11   C1=-3./2./PI*X/R5
      C2=-3./2./PI*X2/R5
      C3=0.
 10   ARG=C1+FT*C2+FA*C3
      DO 14 I=1,JF
      IF(ICALC(I))14,13,13
 13   CONTINUE
      ARGU=1.-(ZB*X-X1(I,1))**2-(ZB*Y*XK)**2
      IF(ARGU.LT.0.) 15,16
 15   FX(I)=1.E-12
      GO TO 17
 16   CONTINUE
      FX(I)=SQRT(ARGU)*ARG
 17   CONTINUE
 14   CONTINUE
      RETURN
      END
        SUBROUTINE PRINC(STRSS,IX,SM,SIM,SMN)
      DIMENSION STRSS(3,3,22)
      C1=STRSS(1,1,IX)+STRSS(2,2,IX)+STRSS(3,3,IX)
      C1=-C1
      C2=STRSS(1,1,IX)*STRSS(2,2,IX)+STRSS(1,1,IX)*STRSS(3,3,IX)+
     1STRSS(2,2,IX)*STRSS(3,3,IX)-STRSS(1,2,IX)**2-
     2STRSS(1,3,IX)**2-STRSS(2,3,IX)**2
      C3=STRSS(1,1,IX)*STRSS(2,2,IX)*STRSS(3,3,IX)+
     12.*STRSS(1,2,IX)*STRSS(2,3,IX)*STRSS(1,3,IX)-
     2STRSS(1,1,IX)*STRSS(2,3,IX)**2-
     3STRSS(2,2,IX)*STRSS(1,3,IX)**2-
     4STRSS(3,3,IX)*STRSS(1,2,IX)**2
      C3=-C3
      CALL CUBIC(C1,C2,C3,S1,S2,S3)
      SM=S1
      IF(S2.GT.SM) SM=S2
```

```
      IF(S3.GT.SM) SM=S3
      SMN=S1
      IF(S2.LT.SMN) SMN=S2
      IF(S3.LT.SMN) SMN=S3
      SIM=S1
      IF(S2.GT.SMN.AND.S2.LT.SM) SIM=S2
      IF(S3.GT.SMN.AND.S3.LT.SM) SIM=S3
      RETURN
      END
        SUBROUTINE CUBIC(C1,C2,C3,S1,S2,S3)
      PI=3.14159
      A=1./3.*(3.*C2-C1**2)
      B=1./27.*(2.*C1**3-9.*C1*C2+27.*C3)
      IF(A.LT.0.) GO TO 3
      S1=S2=S3=0.
      RETURN
 3    CONTINUE
      PHI=ACOS(-B/2./SQRT(-A**3/27.))
      S1=2.*SQRT(-A/3.)*COS(PHI/3.)-C1/3.
      S2=2.*SQRT(-A/3.)*COS(PHI/3.+2.*PI/3.)-C1/3.
      S3=2.*SQRT(-A/3.)*COS(PHI/3.+4.*PI/3.)-C1/3.
      RETURN
      END
        SUBROUTINE ANGLP(STRSS,S1,S2,S3,AN,IX,SIGNA)
      DIMENSION STRSS(3,3,22),AN(3,3)
      S11=STRSS(1,1,IX)
      S12=STRSS(1,2,IX)
      S13=STRSS(1,3,IX)
      S22=STRSS(2,2,IX)
      S23=STRSS(2,3,IX)
      S33=STRSS(3,3,IX)
      ER=1.E-3
      DO 2 I=1,3
      IF(I.EQ.1) S=S1
      IF(I.EQ.2) S=S2
      IF(I.EQ.3) S=S3
      IF(ABS(S11-S).LT.ER) 3,4
 3    AN(I,1)=1.
      AN(I,2)=AN(I,3)=0.
      GO TO 14
 4    IF(ABS(S22-S).LT.ER) 5,6
 5    AN(I,2)=1.
      AN(I,1)=AN(I,3)=0.
      GO TO 14
 6    IF(ABS(S33-S).LT.ER) 7,8
 7    AN(I,3)=1.
      AN(I,1)=AN(I,2)=0.
      GO TO 14
 8    IF(ABS(S12).LT.ER.AND.ABS(S13).LT.ER) 9,10
 10    A=-(S12*S13-(S11-S)*S23)/(S12**2-(S11-S)*(S22-S))
      C11=((-S12*A-S13)/(S11-S))**2+1.+A**2
      AN(I,3)=SIGMA*SQRT(1./C11)
      AN(I,2)=A*AN(I,3)
      AN(I,1)=(-S12*AN(I,2)-S13*AN(I,3))/(S11-S)
      GO TO 14
 9    IF(ABS(S12).LT.ER.AND.ABS(S23).LT.ER) 11,12
 11   A=-(S12*S23-(S22-S)*S13)/(S23**2-(S22-S)*(S33-S))
      C11=((-S12-S23*A)/(S22-S))**2+1.+A**2
      AN(I,1)=SIGMA*SQRT(1./C11)
      AN(I,3)=A*AN(I,1)
      AN(I,2)=(-S23*AN(I,3)-S12*AN(I,1))/(S22-S)
      GO TO 14
 12   CONTINUE
```

```
      A=-(S13*S23-S12*(S33-S))/(S13**2-(S11-S)*(S33-S))
      C11=((-S23-S13*A)/(S33-S))**2+1.+A**2
      AN(I,2)=SIGNA*SQRT(1./C11)
      AN(I,1)=A*AN(I,2)
      AN(I,3)=(-S13*AN(I,1)-S23*AN(I,2))/(S33-S)
14    CONTINUF
2     CONTINUE
      RETURN
      END
        SUBROUTINE RVSTRS(STRSS,AN,AS,TRVM,TMXX,I,SIGN)
      COMMON/F/ ISTRSS,X1(22,1),GNU,ZR,Y,XK,FT,FA,MX
      DIMENSION STRSS(3,3,22),AN(3,22),AS(3,22)
      TRVM=0.
      TMXX=0.
      ER=1.E-3
      DO 1 IAS=1,21
      AS1=-1.+.1*FLOAT(IAS-1)
      IF(ABS(AN(2,I)).LT.ER.AND.ABS(AN(1,I)).LT.ER) 8,9
8     AS3=0.
      AS2=SIGN*SQRT(1.-AS1**2)
      GO TO 13
9     .F(ABS(AN(1,I)).LT.ER.AND.ABS(AN(3,I)).LT.ER) 10,11
10    AS2=0.
      AS3=SIGN*SQRT(1.-AS1**2)
      GO TO 13
11    IF(ABS(AN(2,I)).LT.ER.AND.ABS(AN(3,I)).LT.ER) GO TO 12
      IF(ABS(AN(2,I)).LT.ER) 16,17
16    AS3=-AN(1,I)*AS1/AN(3,I)
      CC=1.-AS1**2-AS3**2
      IF(CC.LT.0.) GO TO 22
      AS2=SIGN*SQRT(CC)
      GO TO 13
17    IF(ABS(AN(3,I)).LT.ER) 18,19
18    AS2=-AS1*AN(1,I)/AN(2,I)
      CC=1.-AS1**2-AS2**2
      IF(CC.LT.0.) GO TO 22
      AS3=SIGN*SQRT(CC)
      GO TO 13
19    IF(ABS(AN(1,I)).LT.ER) 20,21
20    AS2=AN(3,I)*SIGN*SQRT(1.-AS1**2)
      AS3=-AN(2,I)/AN(3,I)*AS2
      GO TO 13
21    A=AN(2,I)**2+AN(3,I)**2
      B=2.*AN(1,I)*AN(3,I)*AS1
      C=AS1**2*AN(1,I)**2+AN(2,I)**2*AS1**2-AN(2,I)**2
      CC=B**2-4.*A*C
      IF(CC.LT.0.) GO TO 22
      AS3=(-B+SIGN*SQRT(CC))/2./A
      AS2=-(AS3*AN(3,I)+AS1*AN(1,I))/AN(2,I)
13    CONTINUE
      TMX=-1.E+20
      TMN=1.E+20
      DO 2 IX=1,MX
      TAU=AN(1,I)*AS1*STRSS(1,1,IX)+AN(2,I)*AS2*STRSS(2,2,IX)
     1+AN(3,I)*AS3*STRSS(3,3,IX)+AN(1,I)*AS2*STRSS(1,2,IX)
     2+AN(2,I)*AS1*STRSS(1,2,IX)+AN(1,I)*AS3*STRSS(1,3,IX)
     3+AN(3,I)*AS1*STRSS(1,3,IX)+AN(2,I)*AS3*STRSS(2,3,IX)
     4+AN(3,I)*AS2*STRSS(2,3,IX)
      IF(TAU.GT.TMX) 3,4
3     TMX=TAU
      AST1=AS1
      AST2=AS2
      AST3=AS3
```

```
4       IF(TAU.LT.TMN) 5,6
5       TMN=TAU
6       CONTINUE
2       CONTINUE
        TRV=TMX-TMN
        IF(ABS(TRV).GT.ABS(TRVM)) TRVM=TRV
        IF(ABS(TMN).GT.ABS(TMX)) TMX=ABS(TMN)
        IF(TMX.GT.TMXX) 23,22
23      TMXX=TMX
        AS(1,I)=AST1
        AS(2,I)=AST2
        AS(3,I)=AST3
22      CONTINUE
1       CONTINUE
        RETURN
12      WRITE(1,15)
15      FORMAT( * SOLUTION NOT APPROPRIATE *)
        RETURN
        END
          SUBROUTINE ANGTRAN(AN,BN,CN,IX)
        DIMENSION AN(3,3),BN(3),CN(3,22)
        CN(1,IX)=BN(1)*AN(1,1)+BN(2)*AN(2,1)+BN(3)*AN(3,1)
        CN(2,IX)=BN(1)*AN(1,2)+BN(2)*AN(2,2)+BN(3)*AN(3,2)
        CN(3,IX)=BN(1)*AN(1,3)+BN(2)*AN(2,3)+BN(3)*AN(3,3)
        RETURN
        END
          SUBROUTINE XPOS
        COMMON/F/ IS,X1(22,1),GNU,Z,Y,XK,FT,FA,MX
        IF(MX.EQ.7) 1,2
1       X1(1,1)=-.8
        X1(2,1)=-.5
        X1(3,1)=-.3
        X1(4,1)=0.
        X1(5,1)=.3
        X1(6,1)=.5
        X1(7,1)=.8
        RETURN
2       IF(MX.EQ.11) 3,4
3       X1(1,1)=-1.
        X1(2,1)=-.9
        X1(3,1)=-.8
        X1(4,1)=-.5
        X1(5,1)=-.3
        X1(6,1)=0.
        X1(7,1)=.3
        X1(8,1)=.5
        X1(9,1)=.6
        X1(10,1)=.9
        X1(11,1)=1.
        RETURN
4       IF(MX.EQ.15) 5,6
5       X1(1,1)=-1.
        X1(2,1)=-1.
        X1(3,1)=-.9
        X1(4,1)=-.8
        X1(5,1)=-.7
        X1(6,1)=-.5
        X1(7,1)=-.3
        X1(8,1)=0.
        X1(9,1)=.3
        X1(10,1)=.5
        X1(11,1)=.7
        X1(12,1)=.8
```

```
      X1(13,1)=.9
      X1(14,1)=1.
      X1(15,1)=1.1
      RETURN
    6 PRINT 10
   10 FORMAT( * MATRIX NOT AVAILABLE * )
      RETURN
      END
```

11.11.12. LS12 IOLCOLC 0000518 LINES PRINTED //// END OF LIST ////